DMD Fast Forward. Published on October 14, 2021 as DOI: 10.1124/dmd.121.000503
This article has not been copyedited and formatted. The final version may differ from this version.

Simulating the Selection of Resistant Cells with Bystander Killing and Antibody Coadministration in Heterogeneous HER2 Positive Tumors

Bruna Menezes[*], Jennifer J. Linderman[*#], Greg M. Thurber[*#]

[*] Department of Chemical Engineering, University of Michigan, Ann Arbor, MI 48109

[#] Department of Biomedical Engineering, University of Michigan, Ann Arbor, MI 48109

DMD Fast Forward. Published on October 14, 2021 as DOI: 10.1124/dmd.121.000503
This article has not been copyedited and formatted. The final version may differ from this version.

Selection of Resistant Cells with Antibody-Drug Conjugates (Short Title)

Bruna Menezes[*], Jennifer J. Linderman[*#], Greg M. Thurber[*#]

[*] Department of Chemical Engineering, University of Michigan, Ann Arbor, MI 48109

[#] Department of Biomedical Engineering, University of Michigan, Ann Arbor, MI 48109

Corresponding Authors:

Jennifer J. Linderman
University of Michigan
2800 Plymouth Rd., Ann Arbor, MI 48109
E-mail: linderma@umich.edu

Greg M. Thurber
University of Michigan
2800 Plymouth Rd., Ann Arbor, MI 48109
E-mail: gthurber@umich.edu

Number of
Text pages: 23
Tables: 0
Figures: 6
References: 57

Number of words
Abstract: 250
Introduction: 801
Discussion: 1673

Abbreviations
Ado-trastuzumab emtansine (T-DM1)
Agent-based model (ABM)
Antibody-dependent cellular cytotoxicity (ADCC)
Antibody-drug conjugate (ADC)
Emtansine (DM1)
Human epidermal growth factor receptor 2 (HER2)
Monomethyl auristatin E (MMAE)
Pharmacodynamics (PD)
Pharmacokinetics (PK)
Trastuzumab-monomethyl auristatin E (T-MMAE)

DMD Fast Forward. Published on October 14, 2021 as DOI: 10.1124/dmd.121.000503
This article has not been copyedited and formatted. The final version may differ from this version.

Abstract

Intratumoral heterogeneity is a leading cause of treatment failure resulting in tumor recurrence. For the antibody-drug conjugate (ADC) ado-trastuzumab emtansine (T-DM1), two major types of resistance include changes in HER2 expression and reduced payload sensitivity, often exacerbated by heterogenous HER2 expression and ADC distribution during treatment. ADCs with bystander payloads such as trastuzumab-monomethyl auristatin E (T-MMAE) can reach and kill adjacent cells with lower receptor expression that cannot be targeted directly with the ADC. Additionally, coadministration of T-DM1 with its unconjugated antibody, trastuzumab, can improve distribution and minimize heterogeneous delivery. However, the effectiveness of trastuzumab coadministration and ADC bystander killing in heterogenous tumors in reducing the selection of resistant cells is not well-understood. Here, we use an agent-based model to predict outcomes with these different regimens. The simulations demonstrate that both T-DM1 and T-MMAE benefit from trastuzumab coadministration for tumors with high average receptor expression (up to 70 and 40% decrease in average tumor volume, respectively), with greater benefit for non-bystander payloads. However, the benefit decreases as receptor expression is reduced, reversing at low concentrations (up to 360 and 430% increase in average tumor volume, respectively) for this mechanism that impacts both ADC distribution and efficacy. For tumors with intrinsic payload resistance, coadministration uniformly exhibits better efficacy than ADC monotherapy (50-70% and 19-36% decrease in average tumor volume for T-DM1 and T-MMAE, respectively). Finally, we demonstrate that several regimens select for resistant cells at clinical tolerable doses, highlighting the need to pursue other mechanisms of action for durable treatment responses.

DMD Fast Forward. Published on October 14, 2021 as DOI: 10.1124/dmd.121.000503
This article has not been copyedited and formatted. The final version may differ from this version.

Significance Statement

Experimental evidence demonstrates heterogeneity in the distribution of both ADCs and the target receptor in the tumor microenvironment, which can promote the selection of resistant cells and lead to recurrence. Here we quantify the impact of increasing the antibody dose and/or utilizing bystander payloads in heterogeneous tumors using an agent-based model and highlight the need for alternative cell killing mechanisms to avoid enriching resistant cell populations.

DMD Fast Forward. Published on October 14, 2021 as DOI: 10.1124/dmd.121.000503
This article has not been copyedited and formatted. The final version may differ from this version.

Introduction

One of the main causes of treatment failures for therapies that target HER2 receptors is intratumoral heterogeneity, which typically leads to cancer relapse with a worse prognosis (Rye et al., 2018). The combination of incomplete cell killing and tumor heterogeneity is a widespread problem in chemotherapy that can result in selection of resistant cell populations. Residual tumor cells left from previous treatment are the major cause of tumor recurrence (Allgayer & Aguirre-Ghiso, 2008; J. Li et al., 2015). Finding approaches to eliminate all tumor cells is a challenging task in the development of effective treatments that avoid tumor relapse.

Antibody-drug conjugates (ADCs) such as ado-trastuzumab emtansine (T-DM1), commercially known as Kadcyla®, are a type of targeted therapy approved by the Food and Drug Administration (FDA) for HER2-overexpressing breast cancer relapsed from treatment with trastuzumab (Herceptin®) (Manthri, Singal, Youssef, & Chakraborty, 2019). T-DM1 efficacy has been linked closely to HER2 expression, and its efficacy decreases with a decrease in HER2 expression (Garcia-Alonso, Ocana, & Pandiella, 2020). Recently, Bon *et al.* have shown that patients previously treated with pertuzumab (also a HER2 monoclonal antibody targeting agent) have reduced HER2 receptor availability, making T-DM1 less effective as a second-line treatment for patients previously treated with trastuzumab/pertuzumab as a first line regimen (Bon et al., 2020). Unfortunately, T-DM1 resistance is not limited to HER2 expression, and other forms of resistance such as limited tissue penetration (i.e. a 'binding site barrier'), defective internalization, drug efflux pumps, and reduced lysosomal proteolysis make both acquired and intrinsic resistance a major problem (Barok, Joensuu, & Isola, 2014; Garcia-Alonso et al., 2020; Hamblett et al., 2015; Hunter et al., 2020; Rios-Luci et al., 2017; Staudacher & Brown, 2017). In this study, we focus on two mechanisms of resistance: i) reduced HER2 expression as a

DMD Fast Forward. Published on October 14, 2021 as DOI: 10.1124/dmd.121.000503
This article has not been copyedited and formatted. The final version may differ from this version.

mechanism that impacts both tissue distribution and cellular potency, and ii) payload sensitivity, which impacts cell potency without changing tumor ADC distribution.

New ADC mechanisms and administration regimens have been shown to potentially overcome some of the barriers and resistance mechanisms to treatment. Some ADCs, for example, contain linkers and payloads that are more lipophilic than the DM1-lysine conjugate released by T-DM1, like DM1 (with a cleavable linker) and MMAE (Erickson et al., 2010; Kovtun et al., 2006). These payloads have the ability to enter adjacent cells by crossing the cell membranes once they are released inside ADC-targeted cells. This mechanism of uptake is known as the bystander effect. If the payload reaches a sufficient concentration, adjacent cells that cannot be directly targeted by the ADC may be killed. This has been one strategy to kill cells that are resistant due to lower receptor expression.

In addition to target expression heterogeneity, antibodies distribute heterogeneously due to their fast-binding rates relative to diffusion (Graff & Wittrup, 2003). This effect, first observed early after the advent of monoclonal antibodies (Oldham et al., 1984) and described as a ‘binding site barrier’ by Weinstein and colleagues, (Fujimori, Covell, Fletcher, & Weinstein, 1989) has been seen in multiple solid tumors in the clinic (Eary et al., 1989; Lu, Fakurnejad, et al., 2020; Lu, Nishio, et al., 2020; Scott et al., 2005). An approach to improve heterogenous drug distribution during T-DM1 administration is coadministration with its unconjugated antibody trastuzumab. ADC monotherapy with T-DM1 at a clinical dose (3.6 mg/kg) shows that the drug is localized around blood vessels in solid tumors, and most of the tumor does not receive the treatment (Rhoden & Wittrup, 2012). As shown both in mice and in simulations, coadministration of trastuzumab and T-DM1 can improve penetration and efficacy of these therapeutics in solid tumors (Cornelius Cilliers, Menezes, Nessler, Linderman, & Thurber, 2018;

DMD Fast Forward. Published on October 14, 2021 as DOI: 10.1124/dmd.121.000503
This article has not been copyedited and formatted. The final version may differ from this version.

Menezes, Cilliers, Wessler, Thurber, & Linderman, 2020). At the same time, this coadministration reduces the number of payloads in targeted cells (which is important for cell killing (F. Li et al., 2016)), thereby making these cells theoretically more susceptible to continued growth and division. However, it is not known how antibody coadministration and/or ADCs with bystander effects might influence the selection of more resistant cells, which can potentially alter the risk of tumor relapse.

Here, we use a validated agent-based model described previously (Menezes et al., 2020) to quantify how ADCs with bystander payloads modulate efficacy in heterogeneous solid tumors, both with and without coadministered antibody, specifically focusing on overall efficacy and selection of resistant cells. In particular, we ask three questions: 1) How do carrier doses and bystander effects (MMAE vs. SMCC-DM1) impact the distribution, uptake, and efficacy of ADC treatment in tumors with heterogeneous HER2 expression? 2) Do carrier doses and bystander effects show the same influence on efficacy in heterogeneous tumors when cell sensitivity to the payload does not impact tumor distribution? And 3) How do different coadministration regimens affect the selection of resistant cells, which could lead to resistant tumor relapse?

DMD Fast Forward. Published on October 14, 2021 as DOI: 10.1124/dmd.121.000503
This article has not been copyedited and formatted. The final version may differ from this version.

Materials and Methods

We extended our hybrid agent-based model (ABM) framework introduced previously (Menezes et al., 2020) to incorporate additional physical and biological phenomena. Briefly, the model is comprised of cells and blood vessels that behave based on probabilistic rules and their microenvironment. The previous model described: plasma dynamics (clearance and payload deconjugation), drug dynamics (intracellular processing for non-bystander payloads), and cell dynamics (e.g., cell division and cell death) that impact the tumor volume in our simulations. Cells change their state from alive to dead based on the concentration of payload bound to microtubules inside of the cell. A description of our model for the plasma dynamics, drug dynamics, and agent dynamics (cancer cell and blood vessel dynamics) can be found in the Supplement (Equations S.1-S.15 and accompanying text).

Here, the model is extended to include: 1) angiogenesis, allowing us to look at treatment over longer periods of time, 2) heterogeneous receptor expression and/or sensitivity of cancer cells to payloads, and 3) bystander payloads capable of diffusing to nearby cells. These additional features allow us to compare coadministration of T-DM1 and T-MMAE with trastuzumab in different tumor environments (Figure 1).

Simulation Environment and Framework

The model was constructed in C++ with Boost (distributed under the Boost software license – available at www.boost.org). The graphical user interface (GUI) was built using the Qt framework (open-source, distributed under GPL – available at qt.digia.com). Efficient linking and solution of our hybrid multiscale ABM followed the principles described in (Cilfone, Kirschner, & Linderman, 2015) with more details in (Menezes et al., 2020).

DMD Fast Forward. Published on October 14, 2021 as DOI: 10.1124/dmd.121.000503
This article has not been copyedited and formatted. The final version may differ from this version.

The model is a 2D representation of a tumor section that contains blood vessels and several thousand cells. The cells and blood vessels have different states, i.e., alive or dead for cells and functional and non-functional for vessels, and they occupy specific positions on the simulation grid. Each cell occupies a volume of 2 x 10^{-12} L (12.6 μm on a side), and the initial tumor, which has about 1940 cells, is assumed to represent an initial tumor volume range of 200-300 mm^3. ADCs enter the tumor through active blood vessels, and the functional vessel density changes based on the tumor size. Cells were assigned either 1 million receptors/cell (similar to sensitive cell lines like NCI-N87) or 50K receptors/cell (similar to resistant cell lines like JIMT-1) (Le Joncour et al., 2019), and the fraction of cells in each category could be varied. Placement of cells with either receptor number was random on the grid.

ADC Dynamics with Bystander Effects

For distribution studies, drugs are administered as a single administration on day 0, and their dynamics inside the host are described with ordinary and partial differential equations. We previously described drug dynamics with bystander effects within a Krogh cylinder model, which assumes all cells have identical properties, (Eshita Khera, Cilliers, Bhatnagar, & Thurber, 2018) and we use these same equations (with a more sophisticated geometry) in our ABM model here. Briefly, as shown in Supplement Figure S.1. T-DM1, T-MMAE, and trastuzumab are cleared from the plasma biexponentially, while they can at the same time extravasate into the tumor, diffuse through the interstitial tissue, bind to HER2 receptors, and internalize. After ADCs are degraded in lysosomes, the payloads Lys-SMCC-DM1 (referred to as "DM1" henceforth) from T-DM1 and MMAE from T-MMAE enter the cytoplasm and either bind to

DMD Fast Forward. Published on October 14, 2021 as DOI: 10.1124/dmd.121.000503
This article has not been copyedited and formatted. The final version may differ from this version.

microtubules or leave the cell. Both payloads in the interstitial tumor tissue also have the ability to enter cancer cells directly, but at different rates determined by their individual properties.

Vessel Dynamics

While tumors form new blood vessels to sustain tumor growth (angiogenesis), the functional or active vessel density is also known to decrease with increasing tumor size (Hilmas & Gillette, 1974; Williams et al., 1988). In our model, grid locations for blood vessels (functional and non-functional) were identified before the start of simulations. The initial densities of total blood vessels and active blood vessels were calibrated as described in (Menezes et al., 2020). At each agent time step, new blood vessels can become functional as tumor size increases, but the overall vessel density (vessels per tumor volume) decreases (i.e. the tumor volume grows faster than vessel density). This is done by calculating the fraction of active blood vessels at each agent time step and comparing it with the tumor volume at that time and with its initial fraction of active blood vessels set at the beginning of the simulation as shown in Equation 1:

$$fr_t = fr_o \left(\frac{V}{V_0}\right)^{-a} \quad (1)$$

where fr_t is the active fraction of blood vessels at the agent time step, fr_o is the active fraction of blood vessels assigned at the beginning of the simulation, V is tumor volume at the agent time step (mm^3), and V_0 is the initial tumor volume (mm^3). The parameter a was fit to experimental data and has a value of 0.28 (Supplement Fig S.2) (Hilmas & Gillette, 1974). With this method, the overall decrease in active vessel density that occurs at the same time that new blood vessels are formed during the increase in tumor volume is captured.

DMD Fast Forward. Published on October 14, 2021 as DOI: 10.1124/dmd.121.000503
This article has not been copyedited and formatted. The final version may differ from this version.

Cell Dynamics and Model Calibration

Cells proliferate and die as the simulation progresses. All cells in the tumor in a particular simulation proliferate with the same doubling time, with doubling times chosen from 5 to 17 days based on calibration to experimental data (Cornelius Cilliers et al., 2018). Cancer cells change their states from alive to dead based on the concentration of payloads bound to microtubules inside the cell. The probability of cell killing per agent time step is:

$$P_{kill} = \frac{P_{max}\,[P_b]}{K_m + [P_b]} \quad (2)$$

where P_{max} is the maximum probability for cell killing, $[P_b]$ is the concentration of payload bound to microtubules in nM, and K_m is the Michaelis-Menten constant in nM.

In vivo efficacy in a xenograft model

All animal studies were conducted according to University of Michigan Institutional Animal Care and Use Committee. For fractionated dosing, NCI-N87 cells were purchased from ATCC and grown at 37°C with 5% CO in RPMI1640 growth medium supplemented with 10% (v/v) FBS, 50 U/mL penicillin, and 50 μg/mL streptomycin. Mycoplasma testing was performed annually using the Mycoalert Testing Kit (Thermo Fisher Scientific, NC971983). For the xenograft studies, 5 x 10^6 NCI-N87 cells were inoculated in the rear flank of 4–8-week-old female nude (Foxn1 nu/nu) mice from Jackson Laboratories. Tumors were measured with calipers every other day, and the tumor volume was calculated as length x width^2 / 2. When tumors reached approximately 250 mm^3, 3 doses of T-DM1 at 2.4mg/kg were given at days 0, 7, and 14. Tumors were monitored until the tumor reached 2000 mm^3, or until the tumor ulcerated.

DMD Fast Forward. Published on October 14, 2021 as DOI: 10.1124/dmd.121.000503
This article has not been copyedited and formatted. The final version may differ from this version.

Results

Model Calibration and Validation

This model used pharmacokinetic parameters estimated based on physicochemical properties and previously published by Khera et al(Eshita Khera et al., 2018) (see Table S.1 and S.2). Cell doubling time was calibrated to (Cornelius Cilliers et al., 2018) as previously shown in (Menezes et al., 2020), giving a range of 5 to 17 days. The cell killing parameters P_{max} and K_m were herein calibrated and validated for DM1 (T-DM1) and MMAE (T-MMAE) using experimental data from Cilliers *et al.* (Cornelius Cilliers et al., 2018) and Singh *et al.* (Singh, Guo, et al., 2020; Singh, Seigel, et al., 2020) along with *CaliPro*, our calibration protocol for parameter estimation (Joslyn, Kirschner, & Linderman, 2020). For DM1, cell killing calibration is shown in Fig. S.3.A with P_{max} and K_m 0.0014 and 800 respectively and validated in Fig. S.3.B-D. For MMAE, P_{max} and K_m were 0.006 and 600 for calibration as shown in Fig. S.4.A and validated in Fig. S.4.B-D.

Once the model was calibrated and validated to the pharmacodynamic data, the results were compared to in vivo efficacy data collected following fractionated dosing with 3 doses of 2.4 mg/kg of T-DM1 (3x2.4mg/kg) as illustrated in Supplement Fig S.5. As shown in Fig S.5.B, the addition of angiogenesis better fits the experimental data with fractionated doses compared to our previous version of the model (Fig S.5.A) with static vessel distribution.

Bystander Payload Reaches More Cells Albeit at Lower Concentrations per Cell

To compare delivery of bystander and non-bystander payloads to tumor cells, the payload concentrations of MMAE and DM1 were quantified by simulating the distribution and uptake of ADCs and their respective payloads for 3.6 mg/kg of T-DM1 with DAR 3.5 (clinical dose) and

DMD Fast Forward. Published on October 14, 2021 as DOI: 10.1124/dmd.121.000503
This article has not been copyedited and formatted. The final version may differ from this version.

1.8 mg/kg of T-MMAE with DAR 4. The results shown in Figure 2 reflect the maximum peak that occurs at day 1 (24 hours) for ADCs bound to the cell surface and at day 4 for microtubule-bound payload. T-DM1 at 3.6 mg/kg reaches more cells at day 1 than T-MMAE at 1.8 mg/kg, consistent with increased penetration of a higher antibody dose. However, the MMAE payload reaches more cells at day 4 than DM1 (Fig 2.C, Fig 2.D), consistent with previous results from our Krogh cylinder model and as expected given the bystander effects for MMAE (Ilovich et al., 2018; Eshita Khera et al., 2018).

The single cell analysis capabilities of our ABM were used to quantify the penetration of MMAE in comparison to DM1, as measured by the percentage of cells with high payload concentrations (≥150nM), moderate concentrations (150nM > x ≥ 1nM), and low concentrations (< 1nM) (F. Li et al., 2016) (Fig 2.E). We also examined two additional scenarios (3mg/kg and DAR3 for both T-DM1 and T-MMAE to match the dose and DAR for a more direct comparison of the ADCs), as shown in Supplemental Fig S.6. For T-MMAE administration, all cells are reached by MMAE, and the majority of cells receive concentrations between 150nM and 1nM. In contrast, DM1 reaches fewer cells, and the majority of targeted cells receive concentrations higher than 150nM. Many cells in T-DM1 administration receive very little DM1, demonstrating a more heterogeneous distribution (Fig 2.E). These data capture the bystander effect of payloads such as MMAE that reach more cells although with lower concentrations than a non-bystander payload, a consequence of the payload's lipophilicity and ability to diffuse into adjacent cells.

Antibody Coadministration Reduces Efficacy in Tumors with Low Receptor Expression

To compare how coadministration of trastuzumab with T-DM1 or T-MMAE impacts the efficacy in tumors with cell populations with heterogeneous receptor expression (versus a base

DMD Fast Forward. Published on October 14, 2021 as DOI: 10.1124/dmd.121.000503
This article has not been copyedited and formatted. The final version may differ from this version.

case of uniform high expression), we simulated tumors with varying fractions of cells with 1 million or 50,000 receptors per cell and treated with trastuzumab to ADC dose ratios of 0:1, 3:1, and 8:1, dosing every 21 days (day 0, 21, and 42). The average tumor volumes at 50 days for administration of T-DM1 at 3.6 mg/kg (DAR 3.5) and T-MMAE at 1.8 mg/kg (DAR 4) are shown in Figure 3. In tumors with 60% - 100% of cells expressing 1M receptors, adding a carrier dose improves the efficacy for T-DM1 and for T-MMAE (up to 70 and 40 % decrease in average tumor volume, respectively). In tumors with a majority of cells having lower receptor numbers (0% to 20% with 1M receptors), coadministration reduces efficacy (up to 360 and 430 % increase in average tumor volume for T-DM1 and for T-MMAE, respectively), and administration of ADC alone is more efficacious. The poor efficacy of coadministration with heterogeneous expression is similar to that for tumors with uniformly low receptor expression. When most cells express only a low number of receptors, ADCs distribute more evenly in the tumor than for high receptor expression, increasing efficacy. Adding unconjugated antibody to the regimen (coadministration) puts the unconjugated antibody in competition with ADCs, and cells with fewer receptors do not internalize sufficient ADC for cell killing, lowering efficacy.

The trade-off between improved tissue distribution (pharmacokinetics) and targeted cell killing (pharmacodynamics) is highlighted in the shift of cell populations with high, moderate, and low levels of payload uptake. Supplemental Fig S.7 quantifies the percentages of cells with different payload concentrations. These simulations show an increase in the fraction of cells with high payload delivery for the 0:1 regimen as the average receptor expression drops and tissue penetration increases versus a decrease in payload delivery for the 8:1 regimen.

Bystander Effects Mitigate Loss in Efficacy from Coadministration at Low Receptor Expression

DMD Fast Forward. Published on October 14, 2021 as DOI: 10.1124/dmd.121.000503
This article has not been copyedited and formatted. The final version may differ from this version.

To better understand the role of MMAE bystander effects on T-MMAE efficacy, we simulated the distribution and efficacy of T-MMAE while artificially removing the payload's ability to enter adjacent cells. We performed simulations with varying receptor expression, similar to Figure 3, and we set the internalization rate constant of MMAE to enter adjacent cells to zero (k_{inp}=0) as shown on Figure 4. Comparing the distribution of Figure 4.E with control (Figure 4.B), the elimination of payload entering adjacent cells reduces the MMAE uptake in bystander cells, as expected. The tumor growth curves show modestly improved responses when bystander effects are included, with significant improvement for high coadministered doses with low receptor expression, where bystander effects help retain payload concentrations at an effective level.

Coadministration Improves Efficacy in Tumors with Intrinsically Resistant Cells

Not all mechanisms of drug sensitivity impact distribution. We simulated tumors with cell populations that are naturally more resistant to treatment (using a higher value of Km; Eq. 2) and predicted how coadministration affects tumor response. For these cells, Km was doubled (Km=2x) or quadrupled (Km=4x), and simulations with varying percentages of more sensitive cell populations, with and without coadministration, are shown in Figure 5. For T-DM1, 3:1 or 8:1 antibody co-administration improves efficacy compared to ADC alone, increasing the percentage of resistant cells uniformly reduces efficacy (Figure 5.A and B). For T-MMAE, coadministration for tumors with a high fraction of sensitive cells also shows the benefit of the carrier dose. However, as the percentage of cells with intrinsic resistance increases, the benefit of the carrier dose is less evident. This is due to the high 'dilution' of T-MMAE with trastuzumab,

DMD Fast Forward. Published on October 14, 2021 as DOI: 10.1124/dmd.121.000503
This article has not been copyedited and formatted. The final version may differ from this version.

which affects the ability to kill those more resistant cells that require a higher concentration of the payload despite better tissue penetration reaching more cells.

Regimens with Greater Efficacy Can Select for More Resistant Cells

Next, we questioned whether bystander or non-bystander payloads and/or different coadministrations could select for a small number of less sensitive cells that might then repopulate the tumor. Simulations were performed in which the initial tumor was composed of 1% cells with lower receptor expression (Figure 6.A-F), or with intrinsic resistance (value of Km 2x) (Figure 6.G-L). Simulations were conducted for 100 days with dosing every 3 weeks to provide time for the resistant cells to overtake the tumor, resulting in larger tumor sizes. In general, as the ratio of trastuzumab to ADC increases, efficacy is increased for both T-DM1 and T-MMAE administration in heterogenous receptor expressing tumors. However, resistant cells become a larger percentage of the tumor in several scenarios, showing the selection of resistant cells. The selection is highest for a non-bystander payload (T-DM1) at the highest coadministration dose (8:1). Notably, this is also the most effective treatment. T-MMAE had improved efficacy with higher coadministration for tumors with differences in receptor expression, but it also showed selection of resistant cells with coadministration. These simulations indicate that bystander killing alone may not be sufficient to prevent the outgrowth of resistant cells at clinical doses, with or without a carrier dose.

MMAE exhibits bystander effects that allow the drug to diffuse more homogeneously through the tumor, but it also decreases the single-cell uptake. For intrinsic resistance that requires a higher concentration of the payload, T-MMAE here at 1.8mg/kg dose was not

DMD Fast Forward. Published on October 14, 2021 as DOI: 10.1124/dmd.121.000503
This article has not been copyedited and formatted. The final version may differ from this version.

effective. Since bystander effects result in lower concentrations in cells than directly targeted cells, many of the intrinsically resistant cells distant from vessels do not receive a lethal dose.

Another important observation in these data is that a large number of simulations (e.g. 100) were needed to discern trends in the results. When only 10 simulations were used, the trends seen in Figure 6 are masked by tumor variability (data not shown). This suggests that many samples must be taken to identify the most effective treatment, which may not be feasible with animal experiments alone. These results highlight the need for computational approaches to complement experimental results to better predict clinical outcomes.

DMD Fast Forward. Published on October 14, 2021 as DOI: 10.1124/dmd.121.000503
This article has not been copyedited and formatted. The final version may differ from this version.

Discussion

The clinical success of ADCs has improved in the past few years, including the increased reliance on bystander payloads and higher antibody doses. The main goal of next generation ADCs is to improve the therapeutic index of these drugs by increasing efficacy while maintaining relative safety (Coats et al., 2019). This could be achieved by: 1) increasing the delivery to more cells within the tumor, 2) utilizing bystander payloads with balanced physicochemical properties to reach nearby cells at sufficient concentrations while avoiding extensive tumor washout, and 3) driving immune responses to leverage additional mechanisms of cell killing. In this work, we concentrated on the first two approaches with a particular focus on heterogeneous tumors. Overcoming ADC delivery challenges such as the binding site 'barrier' and heterogeneous receptor expression requires strategies including the use of bystander payloads and higher antibody doses (e.g. coadministration regimens) in order to reach cells that may not be directly targeted by ADCs like T-DM1(Garcia-Alonso et al., 2020; Ocana, Amir, & Pandiella, 2020; Yardley et al., 2015). These approaches have the potential to significantly impact responses and may explain the efficacy of trastuzumab deruxtecan in gastric cancer versus T-DM1. While both are approved for use in breast cancer, the former drug is given at higher antibody doses (6.4 versus 3.6 mg/kg), which increases tissue penetration, and contains a bystander payload to reach low-expressing cells given the higher heterogeneity of HER2 expression in gastric cancer (Thuss-Patience et al., 2017).

Here, we used our updated hybrid agent-based model to predict the efficacy of various dosing strategies of ADCs with bystander or non-bystander payloads in heterogeneous tumors (specifically heterogeneous receptor expression and intrinsic cellular resistance). Our model presents an advantage over previous models because it includes single-cell heterogeneity, drug

DMD Fast Forward. Published on October 14, 2021 as DOI: 10.1124/dmd.121.000503
This article has not been copyedited and formatted. The final version may differ from this version.

responses, high-resolution tuning of cancer cell and blood vessel dynamics, and heterogeneous ADC and payload delivery that are not achievable with commonly used compartmental or Krogh cylinder models.

Bystander payloads vary in lipophilicity and potency, affecting both the ADC's PK and PD. For example, MMAE has increased lipophilicity compared to Lys-SMCC-DM1, with a clogD of 2.01 versus 1.21 respectively (Eshita Khera et al., 2018). This changes how easily payloads cross cell membranes, how much they non-specifically adhere to proteins and membranes inside and outside the tumor cells, and the effective diffusion through the tumor tissue. As seen in Figures 2.C and 2.D (and Supplemental Fig. 6.C and 6.D), this helps MMAE to penetrate deeper and more homogeneously into the tissue, while DM1 has a more heterogeneous distribution influenced exclusively by the penetration depth of the intact ADC. MMAE, on the other hand, does not accumulate to sufficient levels for complete cell killing inside cells reached via the bystander effect at the doses given here (1.8mg/kg), but for higher doses like 3.6mg/kg, the payload reaches cells with concentrations shown to be effective (Singh, Guo, et al., 2020; Singh et al., 2016). Other payloads, such as deruxtecan, have shown significant bystander killing at clinically tolerable doses (Ogitani, Hagihara, Oitate, Naito, & Agatsuma, 2016). These agents may be able to better target antigen negative cells than the payloads used here, which is important for clinically heterogeneous tumors (Seol et al., 2012). Singh et al. emphasized the importance of a parallel decline in antigen-positive and antigen-negative cells within a heterogeneous tumor to maintain bystander killing (Singh, Seigel, et al., 2020). The higher efficiency of direct cell killing relative to bystander killing may make this difficult to achieve in practice (Eshita Khera et al., 2018).

DMD Fast Forward. Published on October 14, 2021 as DOI: 10.1124/dmd.121.000503
This article has not been copyedited and formatted. The final version may differ from this version.

Due to MMAE's relatively high potency, reduced efficacy from the bystander escape of the payload and loss in concentration (washout) are only evident in high trastuzumab ratios and in tumors with low total receptor expression (e.g. < 30% 1M, Fig 4F). Other very potent bystander payloads such as PBD and DGN (DNA alkylators) are also very lipophilic and have demonstrated optimal bystander efficiency by balancing the difference between retention and diffusion through cells, which can minimize washout of the drug from the tumor (Eshita Khera et al., 2018; E. Khera et al., 2020). However, these potent payloads must be administered at lower doses than microtubule inhibitors due to their toxicity.

In general, T-DM1 and T-MMAE efficacy benefit from coadministration with trastuzumab for tumors with high receptor expression, but the benefit of coadministration is reduced and eventually lost for tumors with lower receptor expression as shown in Figure 3. Consistent with previous work, coadministration offers advantages for T-MMAE in high expression tumors, since the efficiency of direct cell targeting is greater than bystander killing (Eshita Khera et al., 2018; Singh, Guo, et al., 2020). Figures 3 and 4 highlight the need for a balance between fast escape of the payload versus accumulation in cells to mediate cell death. Approaches that enable fast endosomal/lysosomal escape but prevent cellular escape/washout (similar to the dolaflexin payload) could increase potency by locking the toxic payload inside of the cytosol (Clardy et al., 2018). The higher efficacy of T-DM1 and T-MMAE with increasing numbers of low-expressing cells may seem counter-intuitive. However, this result, where lower receptor expression improves efficacy due to better tissue penetration, has been observed experimentally (Nessler et al., 2020; Ponte et al., 2020).

Other diverse mechanisms of resistance can lead to intrinsic cellular resistance wherein cells require a higher concentration of drug for cell killing (Barok et al., 2014). We performed

DMD Fast Forward. Published on October 14, 2021 as DOI: 10.1124/dmd.121.000503
This article has not been copyedited and formatted. The final version may differ from this version.

simulations to understand how coadministration of antibody with ADCs carrying bystander and non-bystander payload in the presence of these resistant cells modulates efficacy. In general, the results in Figure 5 show that coadministration is better for the vast majority of tumor compositions when the resistance mechanism does not influence tumor distribution. A few tumor compositions with a very high concentration of resistant cells (right side of Figures 5.C and D) show similar efficacy regardless of carrier dosing, but these regimens are ineffective overall. Strategies such as interchanging payloads (van Geel et al., 2015) may be needed to restore cellular sensitivity in these cases. The benefit of the carrier dose is greater for T-DM1 than T-MMAE due to the ability of bystander payloads to partially compensate for heterogeneous tissue penetration. When the resistance mechanism does not influence distribution, the carrier dose is more consistently beneficial with fewer trade-offs.

In these simulations, we also saw that the regimens that led to better efficacy also led to selection of more resistant cells (Fig 6.C). These dynamics highlight fundamental limitations in improving efficacy by only taking into consideration changes in dosing regimens of ADCs. Although these approaches are beneficial for a period of time, tumor reoccurrence could result in a short duration of response (Banerjee et al., 2018) and potentially lead to an even more resistant tumor composition. This work highlights the need to utilize other mechanisms of action and/or treatments, similar to combination therapy used with current chemotherapeutics. This could include efforts to mitigate specific mechanisms of resistance, such as selecting payloads that are less susceptible to drug exporters, or more broadly effective approaches including the stimulation of an immune response.

This model, like other preclinical models, encounters some limitations in the translation to the clinical setting. For example, many clinical tumor parameters are infeasible to measure,

DMD Fast Forward. Published on October 14, 2021 as DOI: 10.1124/dmd.121.000503
This article has not been copyedited and formatted. The final version may differ from this version.

although progress is being made (Lu, Fakurnejad, et al., 2020; Lu, Nishio, et al., 2020), and the translation to the clinic requires estimation of these parameters with adjustment for species (Shah, Haddish-Berhane, & Betts, 2012; Singh & Shah, 2017). Additional features beyond scaling clearance rates are needed to capture human plasma pharmacokinetics of drugs like T-DM1, such as ADC deconjugation, TMDD, and HER2 shedding (Betts et al., 2020). Finally, stromal cells (including immune cells) can play a major role in response (D'Amico et al., 2019; Iwata et al., 2018; Rios-Doria et al., 2017). While these features are not important in this mouse model, and therefore were not included here, they are important for plasma clearance and tumor response in humans.

This last result and the ability of cells to escape payload killing highlight how more effort should be spent on understanding and developing agents capable of immune stimulation, and for this reason, future work with hybrid ABMs should include immune cells and other molecules. In particular, many ADCs have demonstrated immunostimulatory effects, including benefits from combination therapy with checkpoint inhibitors and immune cell agonists. For example, antibody mechanisms of action, such as ADCC, could also help eradicate cells with lower HER2 expression that have lost sensitivity to receptor signaling blockade (Barok et al., 2007). By including these additional dynamics in the tumor microenvironment, these simulations could help guide the overall development of ADC therapies.

Computational approaches provide a powerful tool to aid ADC development when combined with experimental work (Byun & Jung, 2019; Eshita Khera et al., 2018; Maass, Kulkarni, Betts, & Wittrup, 2016; Singh, Seigel, et al., 2020; Vasalou, Helmlinger, & Gomes, 2015). For example, *in vitro* experiments alone lack the tissue penetration issue that animal results and computational methods can capture for better clinical predictions, e.g.(C. Cilliers,

Guo, Liao, Christodolu, & Thurber, 2016; Cornelius Cilliers et al., 2018). Animal experiments also have significant limitations such as high tolerability and faster pharmacokinetics than humans, resulting in overdosing many animal experiments relative to the clinic and obscuring delivery challenges in vivo. Non-human primate toxicity studies are needed for cross-reactivity to ADCs, but these animals lack tumors, so the interplay of toxicity and efficacy cannot be determined (Ponte et al., 2020). These weaknesses and limitations of experiments can be addressed by calibrated and validated computational approaches that can capture the in vitro, in vivo efficacy, toxicity, and scaling challenges in a single system. In addition, computational approaches provide the power to discern trends that may be lost in the noise during animal studies with small cohort sizes. These trends may not appear until later during development when larger studies and/or clinical trials are conducted. In contrast, a large number of simulations (e.g. n = 100) can more efficiently identify trends in the outcomes. This supports the use of computer simulations, especially with ABMs, as an approach to help streamline the development of ADCs.

DMD Fast Forward. Published on October 14, 2021 as DOI: 10.1124/dmd.121.000503
This article has not been copyedited and formatted. The final version may differ from this version.

Acknowledgments

The authors also thank Paul Wolberg for technical assistance.

Authorship Contributions

Participated in research design: Menezes, Linderman, and Thurber

Conducted Simulations: Menezes.

Performed data analysis: Menezes, Linderman, and Thurber

Wrote or contributed to the writing of the manuscript: Menezes, Linderman, and Thurber

Financial Disclosure

No author has an actual or perceived conflict of interest with the contents of this article.

DMD Fast Forward. Published on October 14, 2021 as DOI: 10.1124/dmd.121.000503
This article has not been copyedited and formatted. The final version may differ from this version.

References

Allgayer, H., & Aguirre-Ghiso, J. A. (2008). The urokinase receptor (u-PAR)--a link between tumor cell dormancy and minimal residual disease in bone marrow? *APMIS, 116*(7-8), 602-614. doi:10.1111/j.1600-0463.2008.00997.x

Banerjee, S., Oza, A. M., Birrer, M. J., Hamilton, E. P., Hasan, J., Leary, A., . . . Liu, J. F. (2018). Anti-NaPi2b antibody-drug conjugate lifastuzumab vedotin (DNIB0600A) compared with pegylated liposomal doxorubicin in patients with platinum-resistant ovarian cancer in a randomized, open-label, phase II study. *Ann Oncol, 29*(4), 917-923. doi:10.1093/annonc/mdy023

Barok, M., Isola, J., Palyi-Krekk, Z., Nagy, P., Juhasz, I., Vereb, G., . . . Szollosi, J. (2007). Trastuzumab causes antibody-dependent cellular cytotoxicity-mediated growth inhibition of submacroscopic JIMT-1 breast cancer xenografts despite intrinsic drug resistance. *Mol Cancer Ther, 6*(7), 2065-2072. doi:10.1158/1535-7163.MCT-06-0766

Barok, M., Joensuu, H., & Isola, J. (2014). Trastuzumab emtansine: mechanisms of action and drug resistance. *Breast Cancer Res, 16*(2), 209. doi:10.1186/bcr3621

Betts, A., Clark, T., Jasper, P., Tolsma, J., van der Graaf, P. H., Graziani, E. I., . . . Barletta, F. (2020). Use of translational modeling and simulation for quantitative comparison of PF-06804103, a new generation HER2 ADC, with Trastuzumab-DM1. *J Pharmacokinet Pharmacodyn, 47*(5), 513-526. doi:10.1007/s10928-020-09702-3

Bon, G., Pizzuti, L., Laquintana, V., Loria, R., Porru, M., Marchio, C., . . . Vici, P. (2020). Loss of HER2 and decreased T-DM1 efficacy in HER2 positive advanced breast cancer treated with dual HER2 blockade: the SePHER Study. *J Exp Clin Cancer Res, 39*(1), 279. doi:10.1186/s13046-020-01797-3

Byun, J. H., & Jung, I. H. (2019). Modeling to capture bystander-killing effect by released payload in target positive tumor cells. *Bmc Cancer, 19*(1), 194. doi:10.1186/s12885-019-5336-7

Cilfone, N. A., Kirschner, D. E., & Linderman, J. J. (2015). Strategies for efficient numerical implementation of hybrid multi-scale agent-based models to describe biological systems. *Cell Mol Bioeng, 8*(1), 119-136. doi:10.1007/s12195-014-0363-6

Cilliers, C., Guo, H., Liao, J., Christodolu, N., & Thurber, G. M. (2016). Multiscale modeling of antibody-drug conjugates: connecting tissue and cellular distribution to whole animal pharmacokinetics and potential implications for efficacy. *AAPS J, 18*(5), 1117-1130. doi:10.1208/s12248-016-9940-z

Cilliers, C., Menezes, B., Nessler, I., Linderman, J., & Thurber, G. M. (2018). Improved tumor penetration and single-cell targeting of antibody–drug conjugates increases anticancer efficacy and host survival. *Cancer Research, 78*(3), 758-768. doi:10.1158/0008-5472.Can-17-1638

Clardy, S. M., Yurkovetskiy, A., Yin, M., Gumerov, D., Xu, L., Ter-Ovanesyan, E., . . . Lowinger, T. B. (2018). Abstract 754: Unique pharmacologic properties of Dolaflexin-based ADCs—a controlled bystander effect. *Cancer Research, 78*(13 Supplement), 754-754. doi:10.1158/1538-7445.Am2018-754

Coats, S., Williams, M., Kebble, B., Dixit, R., Tseng, L., Yao, N. S., . . . Soria, J. C. (2019). Antibody-drug conjugates: future directions in clinical and translational strategies to improve the therapeutic Index. *Clin Cancer Res*. doi:10.1158/1078-0432.CCR-19-0272

D'Amico, L., Menzel, U., Prummer, M., Muller, P., Buchi, M., Kashyap, A., . . . Zippelius, A. (2019). A novel anti-HER2 anthracycline-based antibody-drug conjugate induces adaptive anti-tumor immunity and potentiates PD-1 blockade in breast cancer. *J Immunother Cancer, 7*(1), 16. doi:10.1186/s40425-018-0464-1

Eary, J. F., Schroff, R. W., Abrams, P. G., Fritzberg, A. R., Morgan, A. C., Kasina, S., . . . et al. (1989). Successful imaging of malignant melanoma with technetium-99m-labeled monoclonal antibodies. *J Nucl Med, 30*(1), 25-32. Retrieved from http://www.ncbi.nlm.nih.gov/pubmed/2642954

Erickson, H. K., Widdison, W. C., Mayo, M. F., Whiteman, K., Audette, C., Wilhelm, S. D., & Singh, R. (2010). Tumor delivery and in vivo processing of disulfide-linked and thioether-linked antibody-maytansinoid conjugates. *Bioconjug Chem, 21*(1), 84-92. doi:10.1021/bc900315y

Fujimori, K., Covell, D., Fletcher, J., & Weinstein, J. (1989). Modeling Analysis of the Global and Microscopic Distribution of Immunoglobulin G, $F(ab')_2$, and Fab in Tumors. *Cancer Research, 49*, 5656-5663.

Garcia-Alonso, S., Ocana, A., & Pandiella, A. (2020). Trastuzumab Emtansine: Mechanisms of Action and Resistance, Clinical Progress, and Beyond. *Trends Cancer, 6*(2), 130-146. doi:10.1016/j.trecan.2019.12.010

Graff, C. P., & Wittrup, K. D. (2003). Theoretical analysis of antibody targeting of tumor spheroids: importance of dosage for penetration, and affinity for retention. *Cancer Res, 63*(6), 1288-1296. Retrieved from http://www.ncbi.nlm.nih.gov/entrez/query.fcgi?cmd=Retrieve&db=PubMed&dopt=Citation&list_uids=12649189

Hamblett, K. J., Jacob, A. P., Gurgel, J. L., Tometsko, M. E., Rock, B. M., Patel, S. K., . . . Fanslow, W. C. (2015). SLC46A3 Is Required to Transport Catabolites of Noncleavable Antibody Maytansine Conjugates from the Lysosome to the Cytoplasm. *Cancer Res, 75*(24), 5329-5340. doi:10.1158/0008-5472.CAN-15-1610

Hilmas, D. E., & Gillette, E. L. (1974). Morphometric Analyses of the Microvasculature of Tumors During Growth and After X-irradiation. *Cancer, 33*(1), 103-110.

Hunter, F. W., Barker, H. R., Lipert, B., Rothe, F., Gebhart, G., Piccart-Gebhart, M. J., . . . Jamieson, S. M. F. (2020). Mechanisms of resistance to trastuzumab emtansine (T-DM1) in HER2-positive breast cancer. *Br J Cancer, 122*(5), 603-612. doi:10.1038/s41416-019-0635-y

Ilovich, O., Qutaish, M., Hesterman, J. Y., Orcutt, K., Hoppin, J., Polyak, I., . . . Bradley, D. P. (2018). Dual-Isotope Cryoimaging Quantitative Autoradiography: Investigating Antibody-Drug Conjugate Distribution and Payload Delivery Through Imaging. *J Nucl Med, 59*(9), 1461-1466. doi:10.2967/jnumed.118.207753

Iwata, T. N., Ishii, C., Ishida, S., Ogitani, Y., Wada, T., & Agatsuma, T. (2018). A HER2-Targeting Antibody-Drug Conjugate, Trastuzumab Deruxtecan (DS-8201a), Enhances Antitumor Immunity in a Mouse Model. *Mol Cancer Ther, 17*(7), 1494-1503. doi:10.1158/1535-7163.MCT-17-0749

Joslyn, L. R., Kirschner, D. E., & Linderman, J. J. (2020). CaliPro: A Calibration Protocol That Utilizes Parameter Density Estimation to Explore Parameter Space and Calibrate Complex Biological Models. *Cellular and Molecular Bioengineering*. doi:10.1007/s12195-020-00650-z

Khera, E., Cilliers, C., Bhatnagar, S., & Thurber, G. M. (2018). Computational transport analysis of antibody-drug conjugate bystander effects and payload tumoral distribution: implications for therapy. *Molecular Systems Design & Engineering, 3*(1), 73-88. doi:10.1039/c7me00093f

Khera, E., Cilliers, C., Smith, M. D., Ganno, M. L., Lai, K. C., Keating, T. A., . . . Thurber, G. M. (2020). Quantifying ADC bystander payload penetration with cellular resolution using pharmacodynamic mapping. *Neoplasia, 23*(2), 210-221. doi:10.1016/j.neo.2020.12.001

Kovtun, Y. V., Audette, C. A., Ye, Y., Xie, H., Ruberti, M. F., Phinney, S. J., . . . Goldmacher, V. S. (2006). Antibody-drug conjugates designed to eradicate tumors with homogeneous and heterogeneous expression of the target antigen. *Cancer Res, 66*(6), 3214-3221. doi:10.1158/0008-5472.CAN-05-3973

Le Joncour, V., Martins, A., Puhka, M., Isola, J., Salmikangas, M., Laakkonen, P., . . . Barok, M. (2019). A Novel Anti-HER2 Antibody-Drug Conjugate XMT-1522 for HER2-Positive Breast and Gastric Cancers Resistant to Trastuzumab Emtansine. *Mol Cancer Ther, 18*(10), 1721-1730. doi:10.1158/1535-7163.MCT-19-0207

Li, F., Emmerton, K. K., Jonas, M., Zhang, X., Miyamoto, J. B., Setter, J. R., . . . Law, C. L. (2016). Intracellular Released Payload Influences Potency and Bystander-Killing Effects of Antibody-Drug Conjugates in Preclinical Models. *Cancer Res, 76*(9), 2710-2719. doi:10.1158/0008-5472.CAN-15-1795

Li, J., Jiang, E., Wang, X., Shangguan, A. J., Zhang, L., & Yu, Z. (2015). Dormant Cells: The Original Cause of Tumor Recurrence and Metastasis. *Cell Biochem Biophys, 72*(2), 317-320. doi:10.1007/s12013-014-0477-4

Lu, G., Fakurnejad, S., Martin, B. A., van den Berg, N. S., van Keulen, S., Nishio, N., . . . Rosenthal, E. L. (2020). Predicting Therapeutic Antibody Delivery into Human Head and Neck Cancers. *Clin Cancer Res*. doi:10.1158/1078-0432.CCR-19-3717

Lu, G., Nishio, N., van den Berg, N. S., Martin, B. A., Fakurnejad, S., van Keulen, S., . . . Rosenthal, E. L. (2020). Co-administered antibody improves penetration of antibody-dye conjugate into human cancers with implications for antibody-drug conjugates. *Nat Commun, 11*(1), 5667. doi:10.1038/s41467-020-19498-y

Maass, K. F., Kulkarni, C., Betts, A. M., & Wittrup, K. D. (2016). Determination of Cellular Processing Rates for a Trastuzumab-Maytansinoid Antibody-Drug Conjugate (ADC) Highlights Key Parameters for ADC Design. *AAPS J, 18*(3), 635-646. doi:10.1208/s12248-016-9892-3

Manthri, S., Singal, S., Youssef, B., & Chakraborty, K. (2019). Long-time Response with Ado-trastuzumab Emtansine in a Recurrent Metastatic Breast Cancer. *Cureus, 11*(10), e6036. doi:10.7759/cureus.6036

Menezes, B., Cilliers, C., Wessler, T., Thurber, G. M., & Linderman, J. J. (2020). An Agent-Based Systems Pharmacology Model of the Antibody-Drug Conjugate Kadcyla to Predict Efficacy of Different Dosing Regimens. *AAPS J, 22*(2), 29. doi:10.1208/s12248-019-0391-1

Nessler, I., Khera, E., Vance, S., Kopp, A., Qiu, Q., Keating, T. A., . . . Thurber, G. M. (2020). Increased Tumor Penetration of Single-Domain Antibody-Drug Conjugates Improves In Vivo Efficacy in Prostate Cancer Models. *Cancer Res, 80*(6), 1268-1278. doi:10.1158/0008-5472.CAN-19-2295

Ocana, A., Amir, E., & Pandiella, A. (2020). HER2 heterogeneity and resistance to anti-HER2 antibody-drug conjugates. *Breast Cancer Res, 22*(1), 15. doi:10.1186/s13058-020-1252-7

Ogitani, Y., Hagihara, K., Oitate, M., Naito, H., & Agatsuma, T. (2016). Bystander killing effect of DS-8201a, a novel anti-human epidermal growth factor receptor 2 antibody-drug conjugate, in tumors with human epidermal growth factor receptor 2 heterogeneity. *Cancer Sci, 107*(7), 1039-1046. doi:10.1111/cas.12966

Oldham, R. K., Foon, K. A., Morgan, A. C., Woodhouse, C. S., Schroff, R. W., Abrams, P. G., . . . et al. (1984). Monoclonal antibody therapy of malignant melanoma: in vivo localization in cutaneous metastasis after intravenous administration. *J Clin Oncol, 2*(11), 1235-1244. doi:10.1200/JCO.1984.2.11.1235

Ponte, J. F., Lanieri, L., Khera, E., Laleau, R., Ab, O., Espelin, C., . . . Thurber, G. M. (2020). Antibody Co-Administration Can Improve Systemic and Local Distribution of Antibody Drug Conjugates to Increase In Vivo Efficacy. *Mol Cancer Ther*. doi:10.1158/1535-7163.MCT-20-0451

Rhoden, J. J., & Wittrup, K. D. (2012). Dose dependence of intratumoral perivascular distribution of monoclonal antibodies. *J Pharm Sci, 101*(2), 860-867. doi:10.1002/jps.22801

Rios-Doria, J., Harper, J., Rothstein, R., Wetzel, L., Chesebrough, J., Marrero, A., . . . Hollingsworth, R. (2017). Antibody-Drug Conjugates Bearing Pyrrolobenzodiazepine or Tubulysin Payloads Are Immunomodulatory and Synergize with Multiple Immunotherapies. *Cancer Res, 77*(10), 2686-2698. doi:10.1158/0008-5472.CAN-16-2854

Rios-Luci, C., Garcia-Alonso, S., Diaz-Rodriguez, E., Nadal-Serrano, M., Arribas, J., Ocana, A., & Pandiella, A. (2017). Resistance to the Antibody-Drug Conjugate T-DM1 Is Based in a Reduction in Lysosomal Proteolytic Activity. *Cancer Res, 77*(17), 4639-4651. doi:10.1158/0008-5472.CAN-16-3127

Rye, I. H., Trinh, A., Saetersdal, A. B., Nebdal, D., Lingjaerde, O. C., Almendro, V., . . . Russnes, H. G. (2018). Intratumor heterogeneity defines treatment-resistant HER2+ breast tumors. *Mol Oncol, 12*(11), 1838-1855. doi:10.1002/1878-0261.12375

Scott, A. M., Lee, F. T., Jones, R., Hopkins, W., MacGregor, D., Cebon, J. S., . . . Old, L. J. (2005). A phase I trial of humanized monoclonal antibody A33 in patients with colorectal carcinoma: biodistribution, pharmacokinetics, and quantitative tumor uptake. *Clin Cancer Res, 11*(13), 4810-4817. doi:10.1158/1078-0432.CCR-04-2329

Seol, H., Lee, H. J., Choi, Y., Lee, H. E., Kim, Y. J., Kim, J. H., . . . Park, S. Y. (2012). Intratumoral heterogeneity of HER2 gene amplification in breast cancer: its clinicopathological significance. *Mod Pathol, 25*(7), 938-948. doi:10.1038/modpathol.2012.36

Shah, D. K., Haddish-Berhane, N., & Betts, A. (2012). Bench to bedside translation of antibody drug conjugates using a multiscale mechanistic PK/PD model: a case study with brentuximab-vedotin. *J Pharmacokinet Pharmacodyn, 39*(6), 643-659. doi:10.1007/s10928-012-9276-y

Singh, A. P., Guo, L., Verma, A., Wong, G. G., Thurber, G. M., & Shah, D. K. (2020). Antibody Coadministration as a Strategy to Overcome Binding-Site Barrier for ADCs: a Quantitative Investigation. *AAPS J, 22*(2), 28. doi:10.1208/s12248-019-0387-x

Singh, A. P., Maass, K. F., Betts, A. M., Wittrup, K. D., Kulkarni, C., King, L. E., . . . Shah, D. K. (2016). Evolution of Antibody-Drug Conjugate Tumor Disposition Model to Predict Preclinical Tumor Pharmacokinetics of Trastuzumab-Emtansine (T-DM1). *AAPS J, 18*(4), 861-875. doi:10.1208/s12248-016-9904-3

Singh, A. P., Seigel, G. M., Guo, L., Verma, A., Wong, G. G., Cheng, H. P., & Shah, D. K. (2020). Evolution of the Systems Pharmacokinetics-Pharmacodynamics Model for Antibody-Drug Conjugates to Characterize Tumor Heterogeneity and In Vivo Bystander Effect. *J Pharmacol Exp Ther, 374*(1), 184-199. doi:10.1124/jpet.119.262287

Singh, A. P., & Shah, D. K. (2017). Application of a PK-PD Modeling and Simulation-Based Strategy for Clinical Translation of Antibody-Drug Conjugates: a Case Study with Trastuzumab Emtansine (T-DM1). *AAPS J, 19*(4), 1054-1070. doi:10.1208/s12248-017-0071-y

Staudacher, A. H., & Brown, M. P. (2017). Antibody drug conjugates and bystander killing: is antigen-dependent internalisation required? *Br J Cancer, 117*(12), 1736-1742. doi:10.1038/bjc.2017.367

Thuss-Patience, P. C., Shah, M. A., Ohtsu, A., Van Cutsem, E., Ajani, J. A., Castro, H., . . . Kang, Y. K. (2017). Trastuzumab emtansine versus taxane use for previously treated HER2-positive locally advanced or metastatic gastric or gastro-oesophageal junction adenocarcinoma (GATSBY): an international randomised, open-label, adaptive, phase 2/3 study. *Lancet Oncol, 18*(5), 640-653. doi:10.1016/S1470-2045(17)30111-0

van Geel, R., Wijdeven, M. A., Heesbeen, R., Verkade, J. M., Wasiel, A. A., van Berkel, S. S., & van Delft, F. L. (2015). Chemoenzymatic Conjugation of Toxic Payloads to the Globally Conserved N-Glycan of Native mAbs Provides Homogeneous and Highly Efficacious Antibody-Drug Conjugates. *Bioconjug Chem, 26*(11), 2233-2242. doi:10.1021/acs.bioconjchem.5b00224

Vasalou, C., Helmlinger, G., & Gomes, B. (2015). A mechanistic tumor penetration model to guide antibody drug conjugate design. *PLoS ONE, 10*(3), e0118977. doi:10.1371/journal.pone.0118977

Williams, L. E., Duda, R. B., Proffitt, R. T., Beatty, B. G., Beatty, J. D., Wong, J. Y. C., . . . Paxton, R. J. (1988). Tumor Uptake as a Function of Tumor Mass - A Mathematical Model. *Journal of Nuclear Medicine, 29*(1), 103-109. Retrieved from <Go to ISI>://A1988L675000017

Yardley, D. A., Kaufman, P. A., Huang, W., Krekow, L., Savin, M., Lawler, W. E., . . . Bosserman, L. (2015). Quantitative measurement of HER2 expression in breast cancers: comparison with 'real-world' routine HER2 testing in a multicenter Collaborative Biomarker Study and correlation with overall survival. *Breast Cancer Res, 17*, 41. doi:10.1186/s13058-015-0543-x

DMD Fast Forward. Published on October 14, 2021 as DOI: 10.1124/dmd.121.000503
This article has not been copyedited and formatted. The final version may differ from this version.

Footnotes

This work was supported by the National Institutes of Health [Grant R35 GM128819] (GMT); National Institutes of Health [Grant R01 CA196018] multi-PI (G. Luker, S. Takayama, Linderman), and Department of Defense [Grant BC200857] (GMT and JL).

DMD Fast Forward. Published on October 14, 2021 as DOI: 10.1124/dmd.121.000503
This article has not been copyedited and formatted. The final version may differ from this version.

Figure Legends

Figure 1: Model Schematic
(A) The ABM environment is composed of cancer cells with different characteristics (e.g. different number of receptors or sensitivity to treatment) and blood vessels through which therapeutics are delivered. B) The model tests different regimens: 1) single agent administration (top panel) vs coadministration of antibody with ADC (bottom panel) and 2) non-bystander payloads (left column) vs bystander payloads (right column). The model can be used to examine these regimens for cell populations containing resistant cells.

Figure 2: Similar ADC penetration but greater payload distribution of T-MMAE
(A-B) Distribution of T-DM1 (3.6mg/kg with DAR 3.5) and T-MMAE (1.8 mg/kg, DAR 4) bound on the surface of the cancer cells. (C-D) Distribution of DM1 and MMAE bound to microtubules inside the cells. (E) Percentage of cells with high payload concentrations (≥ 150nM), moderate concentrations (150nM > x ≥ 1nM), and low concentrations (< 1nM) at day 4, the time of maximum payload uptake. n=10 simulations, with mean and SEM shown. T-MMAE has no cells with payload concentration lower than 1nM (shown by the grey arrows). Fig S.6 shows the comparison between these two ADCs for the same dose and DAR; both ADCs reach the same number of cells at day 1, but the MMAE payload again reaches more cells at day 4.

Figure 3: Treatment efficacy at 50 days for tumors with heterogeneous receptor expression.
(A) T-DM1 regimens (3.6 mg/kg and DAR 3.5) and (B) T-MMAE regimens (1.8 mg/kg and DAR 4) for tumors with changing percentage of 1M or 50K receptors per cell for administration every 21 days (at day 0, 21, and 42). Data (mean and SEM) is shown for n=100 simulations. As the number of receptors decreases, coadministration of 8:1 antibody reduces efficacy. These data also show the larger benefit of coadministration for ADCs with non-bystander payloads that cannot diffuse deeper into the tissue to partially compensate for heterogeneous distribution. For tumors with uniformly high expression, the addition of 3:1 and 8:1 carrier doses to T-DM1 reduces tumor growth by a larger amount than for T-MMAE.

Figure 4: Artificially removing bystander effects with coadministration changes payload distribution and efficacy
A-C) Distribution and efficacy for regimens with T-MMAE exhibiting the expected bystander killing. D-F) Distribution and Efficacy for regimens of T-MMAE when setting the internalization rate of free MMAE, k_{inp}, to 0 with different coadministration regimens. Simulations show mean and SEM for n=100 simulations. For MMAE payload, the elimination of bystander effects with high coadministrations leads to lower efficacy. Regimens tested are as in Figure 3.

Figure 5: Efficacy of T-DM1 and T-MMAE coadministration regimens when a fraction of cells has less sensitivity to drug.
Regimens with T-DM1 (A-B) or TMMAE (C-D) with coadministration were simulated. Tumors contained varying fractions of cells with intrinsic resistance (K_m=2x or K_m=4x the value in Table S.2). Lower cell payload sensitivity impacts most regimens in a similar fashion, reducing the overall efficacy regardless of the carrier dose or bystander effects. Simulations show mean and SEM for n=100 simulations. Regimens tested are as in Figure 3.

DMD Fast Forward. Published on October 14, 2021 as DOI: 10.1124/dmd.121.000503
This article has not been copyedited and formatted. The final version may differ from this version.

Figure 6: Tumor growth with initial composition of 1% of resistant cells vs sensitive cells for different regimens with T-DM1 or T-MMAE.

(A-F) Coadministration of trastuzumab 0:1, 3:1, 8:1 with T-DM1 (A-C) and T-MMAE (D-F) every three weeks (marked by arrows) initially containing 1% of tumor cells with 50K receptors per cell vs 99% of 1M receptors per cell. (G-L) Coadministration of trastuzumab 0:1, 3:1, 8:1 with T-DM1 (G-I) and T-MMAE (J-L) every three weeks initially containing 1% of cells with higher intrinsic resistance (Km=2x) vs 99% of cell with Km=1x. Km=800nM for T-DM1 and Km=600nM for T-MMAE. Simulations show mean and SEM for n=100 simulations. In most cases, more effective treatments result in a larger fraction of resistant cells.

DMD Fast Forward. Published on October 14, 2021 as DOI: 10.1124/dmd.121.000503
This article has not been copyedited and formatted. The final version may differ from this version.

Figure 1

A.

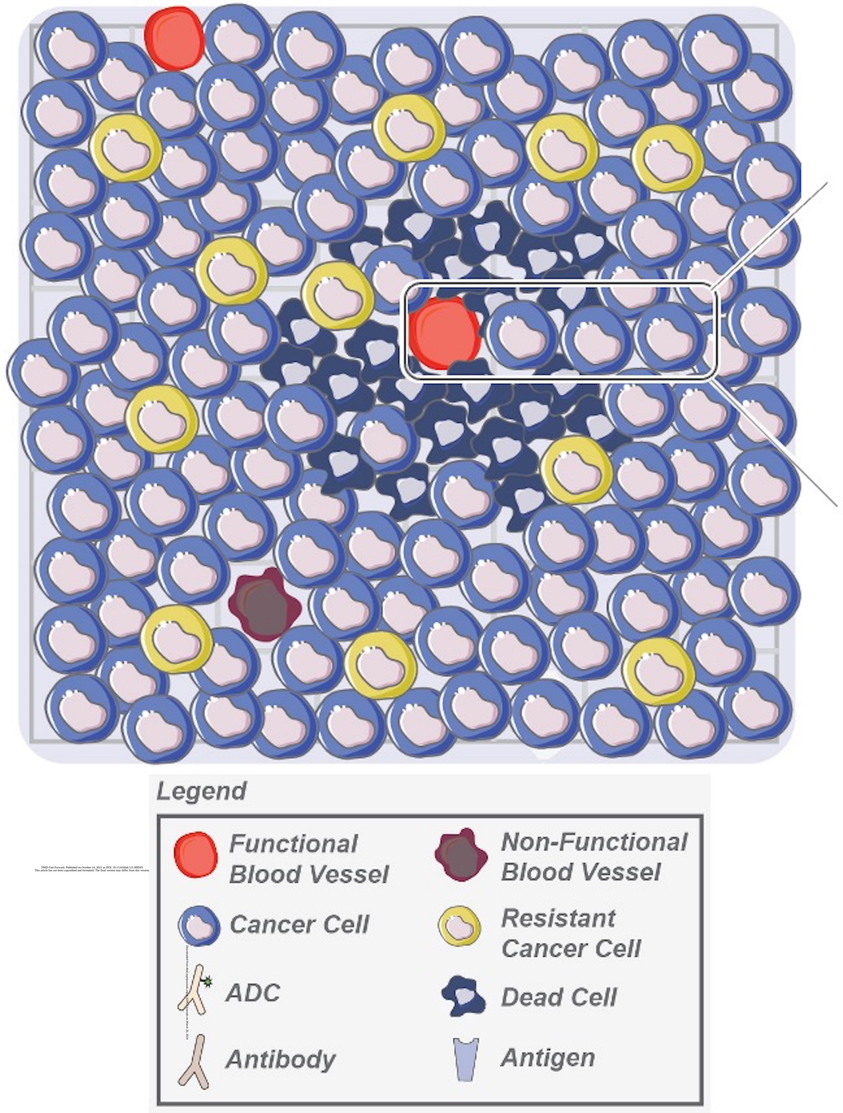
Legend
Functional Blood Vessel
Non-Functional Blood Vessel
Cancer Cell
Resistant Cancer Cell
ADC
Dead Cell
Antibody
Antigen

B.

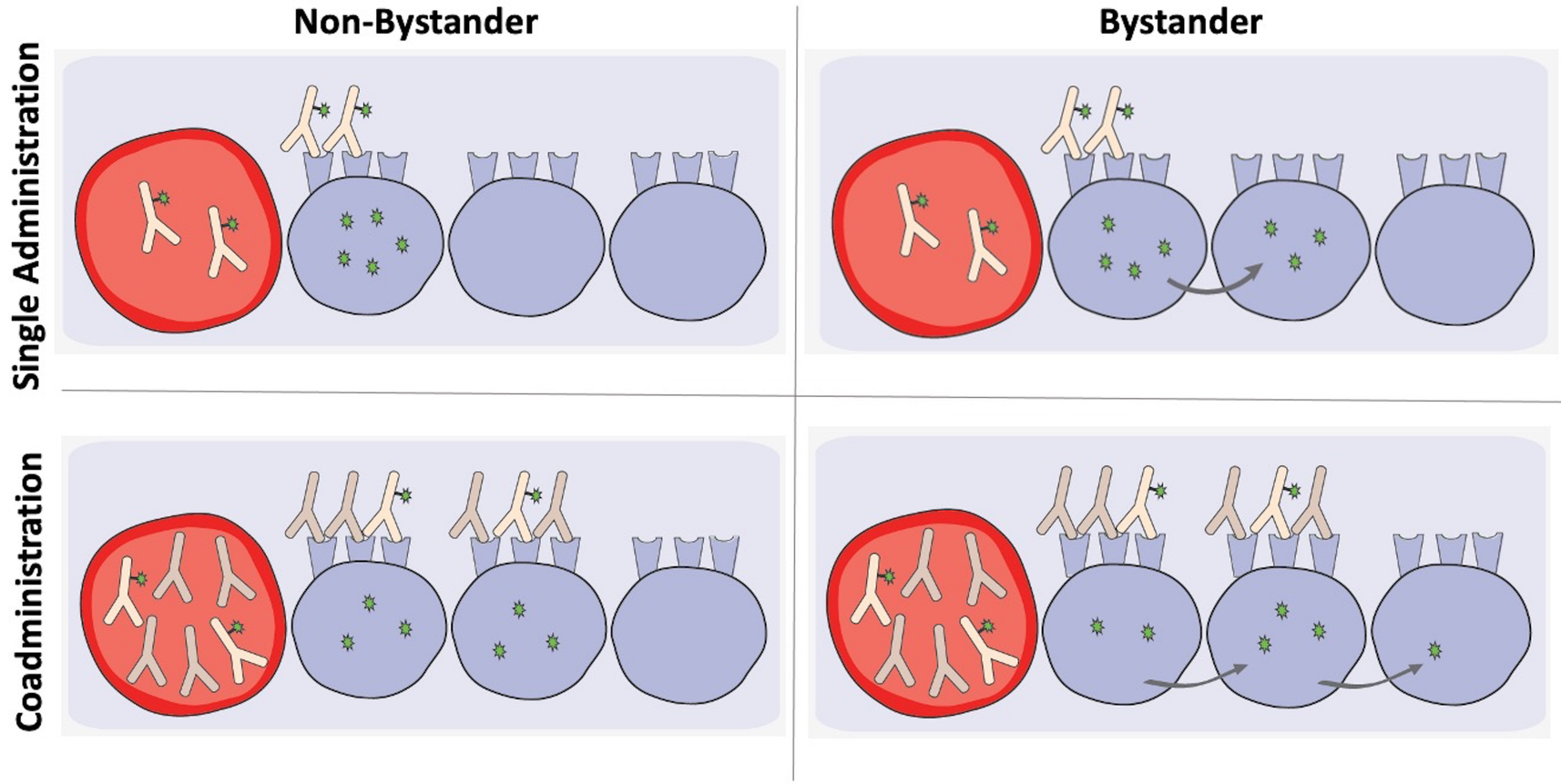
Non-Bystander
Bystander
Single Administration
Coadministration

Figure 2

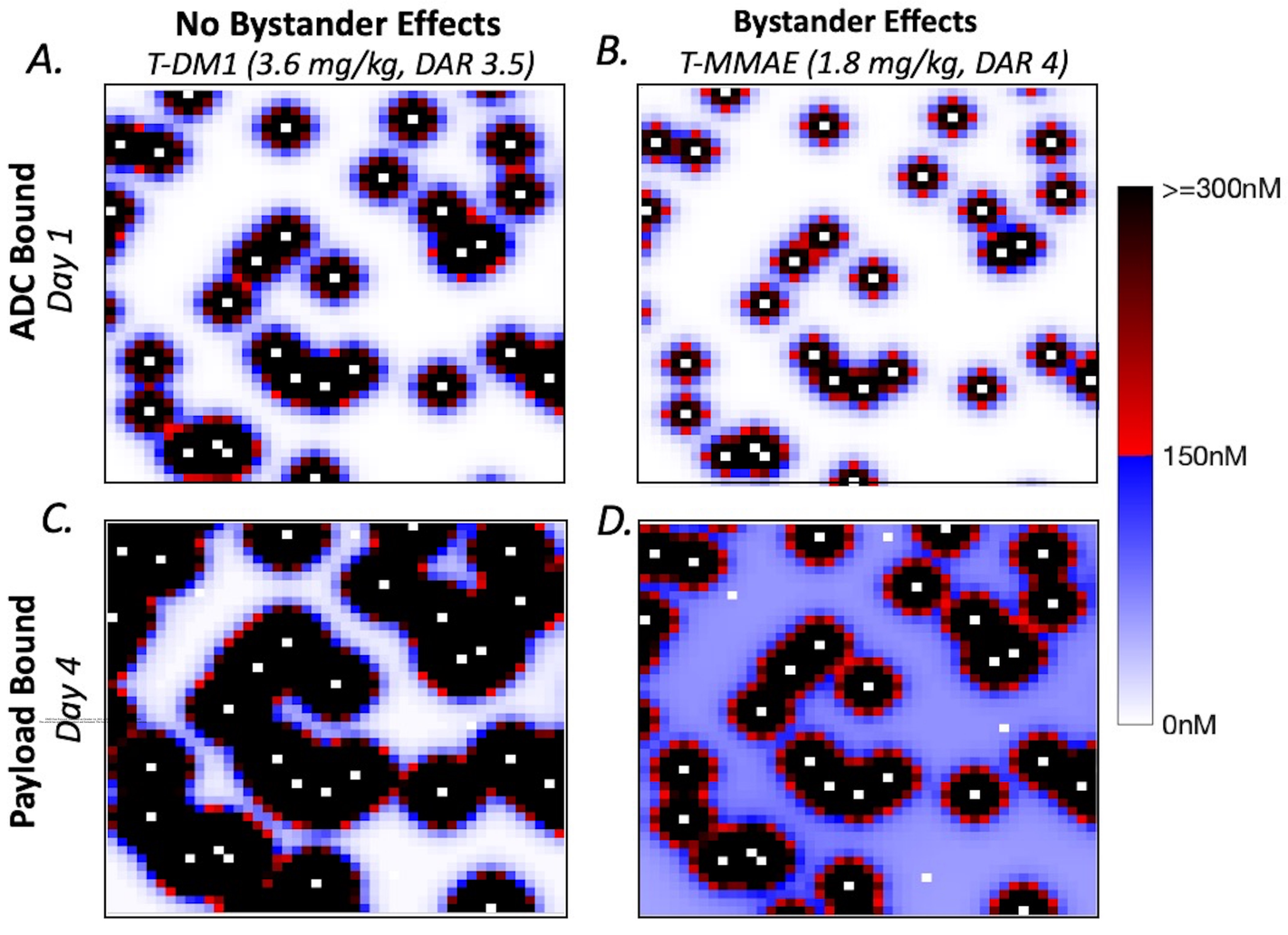

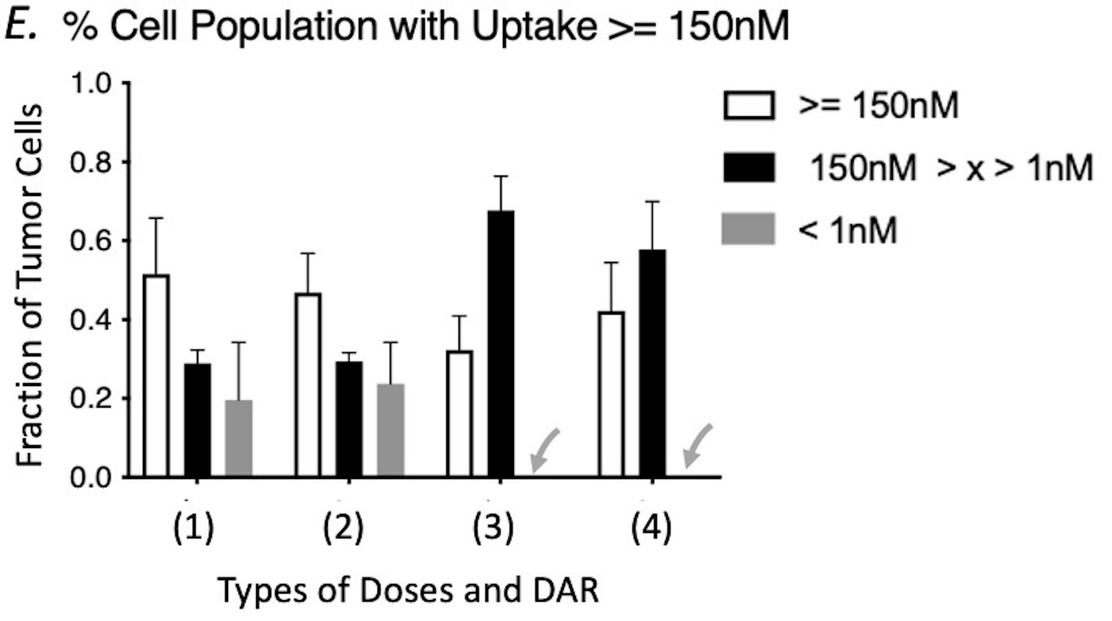

(1) 3.6mg/kg T-DM1, DAR 3.5
(2) 3mg/kg T-DM1, DAR 3
(3) 1.8mg/kg T-MMAE, DAR 4
(4) 3mg/kg T-MMAE, DAR 3

Figure 3

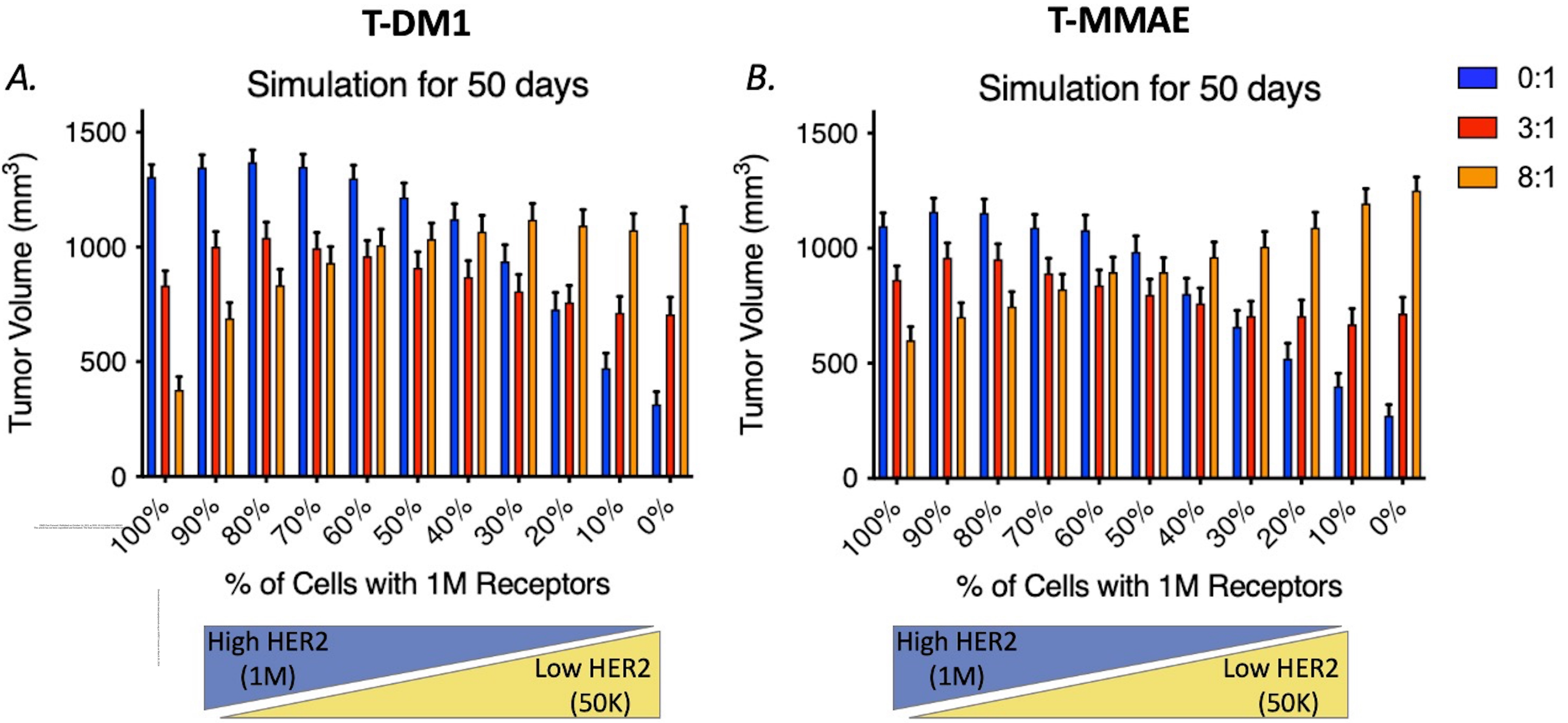
T-DM1
A.
Simulation for 50 days
Tumor Volume (mm3)
1500
1000
500
0
100%
90%
80%
70%
60%
50%
40%
30%
20%
10%
0%
% of Cells with 1M Receptors
High HER2 (1M)
Low HER2 (50K)
T-MMAE
B.
Simulation for 50 days
0:1
3:1
8:1

Figure 4

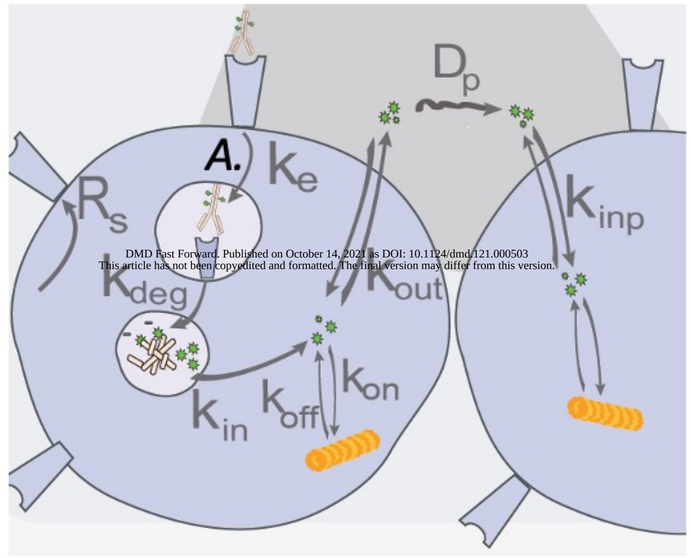

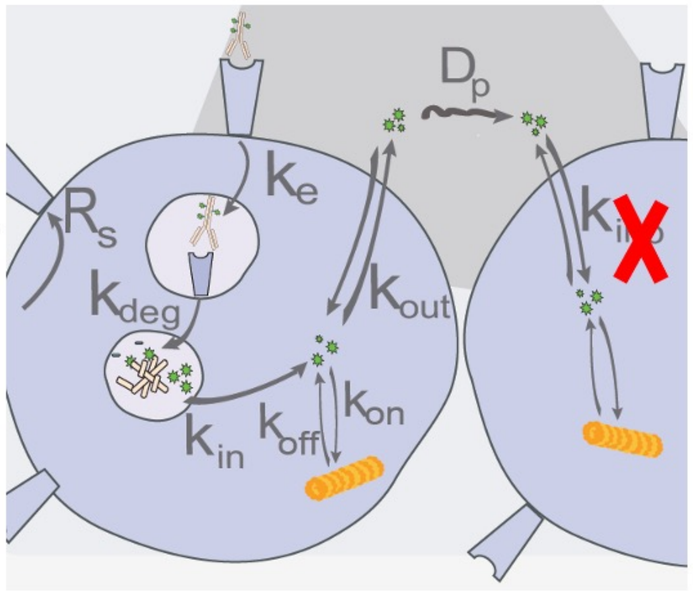

B.

MMAE bound
Single dose (Day 4)

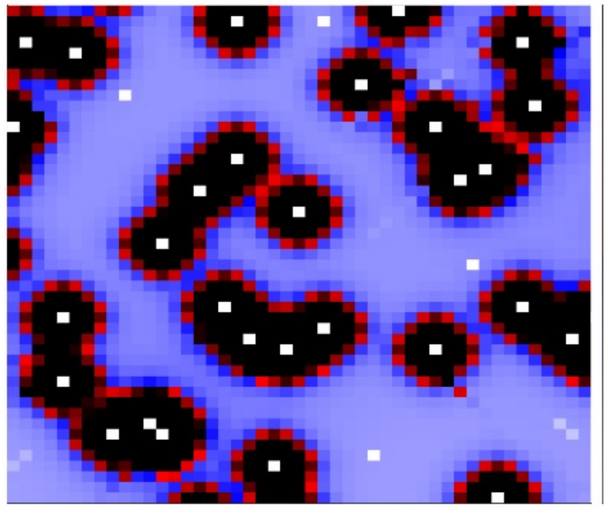

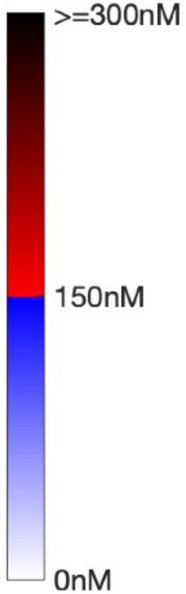

E.

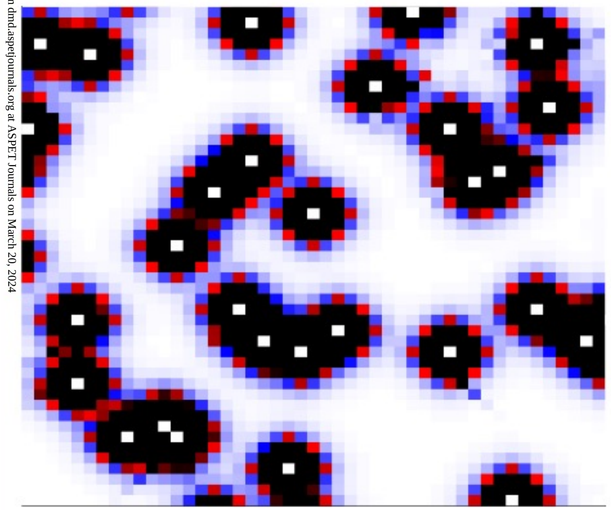

C.

Efficacy

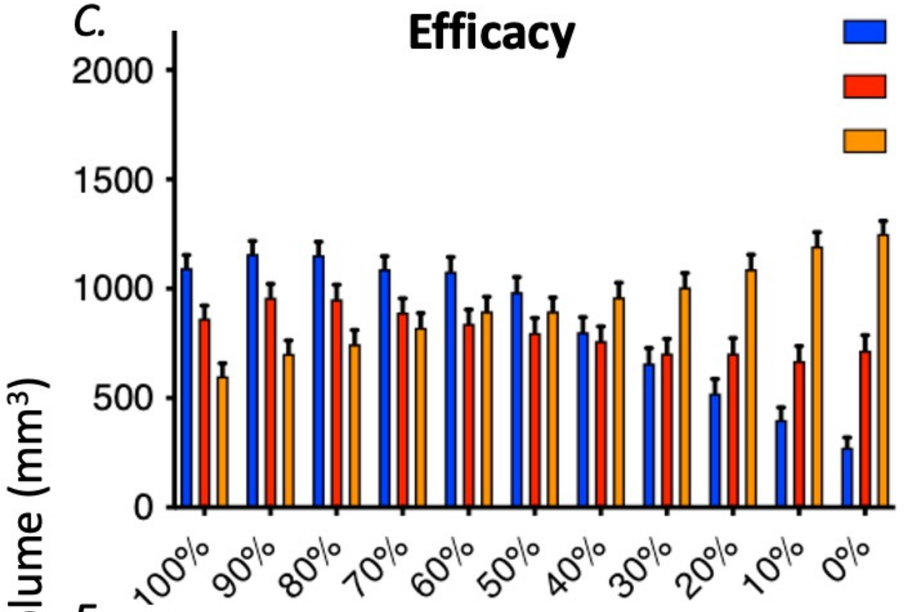

F.

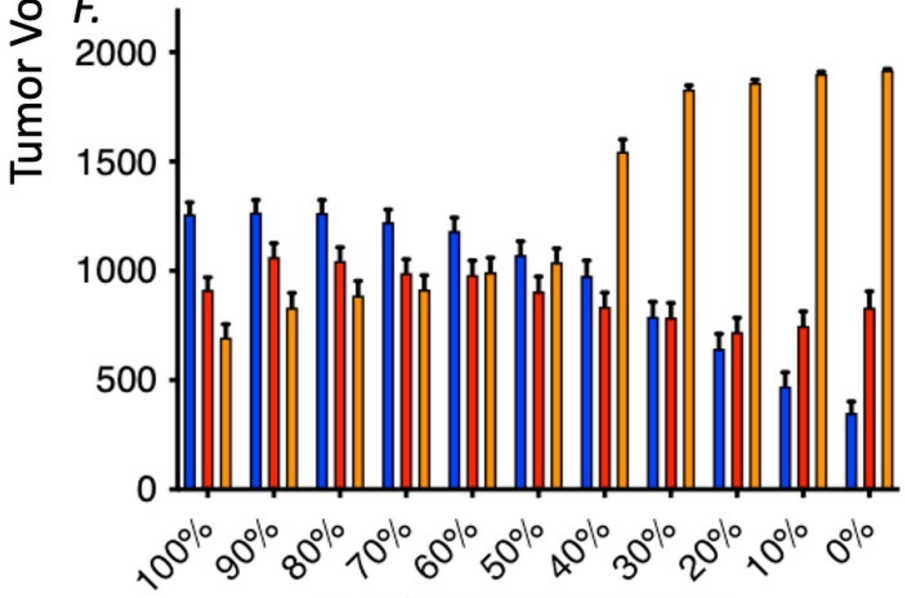

% of Cells with 1M Receptors

Figure 5

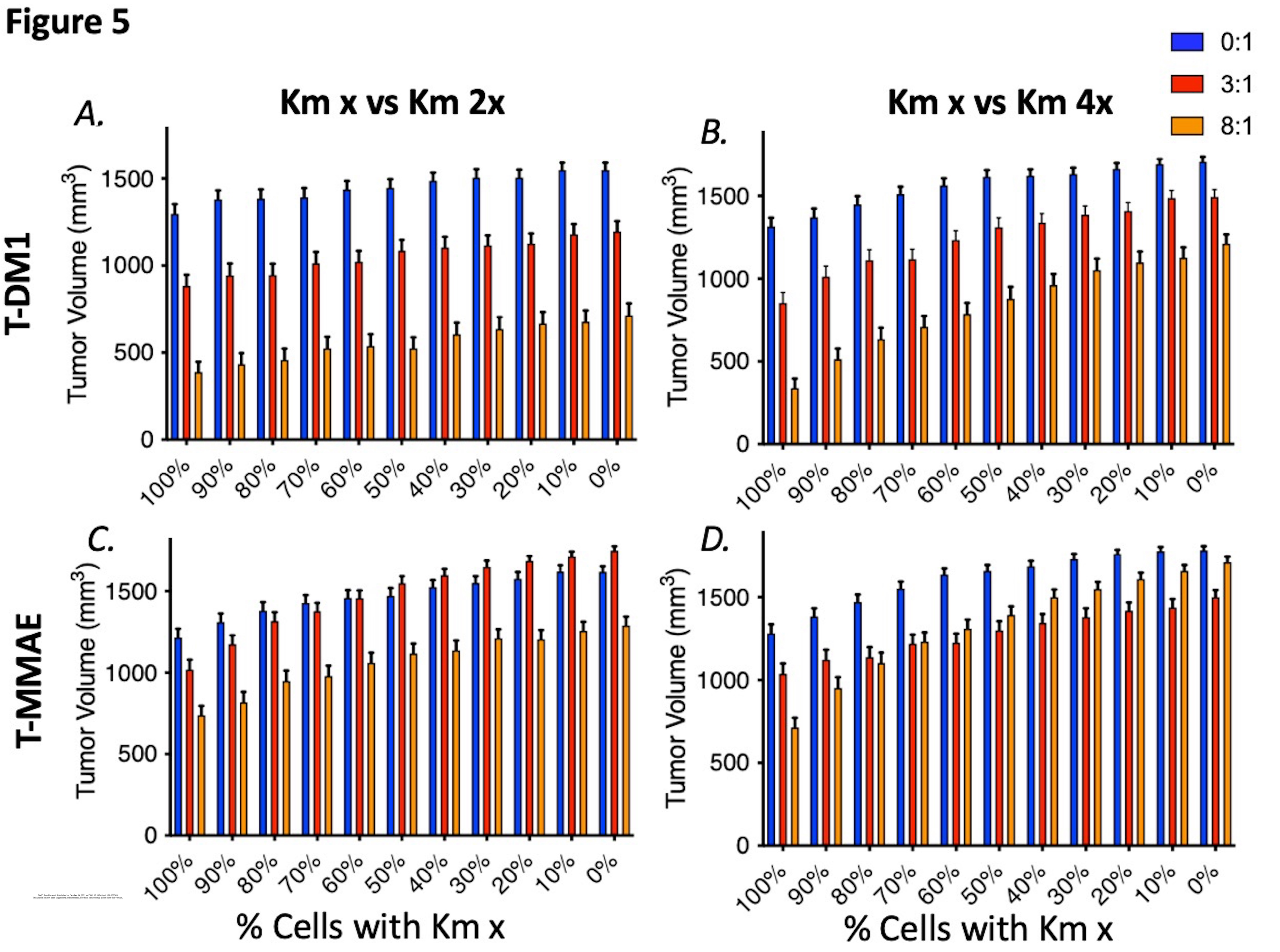
T-DM1
T-MMAE
A.
Km x vs Km 2x
B.
Km x vs Km 4x
C.
D.
0:1
3:1
8:1
Tumor Volume (mm3)
0
500
1000
1500
100%
90%
80%
70%
60%
50%
40%
30%
20%
10%
0%
% Cells with Km x
More Sensitive
(Km = x)
More Resistant
(Km = 2x)
More Sensitive
(Km = x)
More Resistant
(Km = 4x)

Figure 6

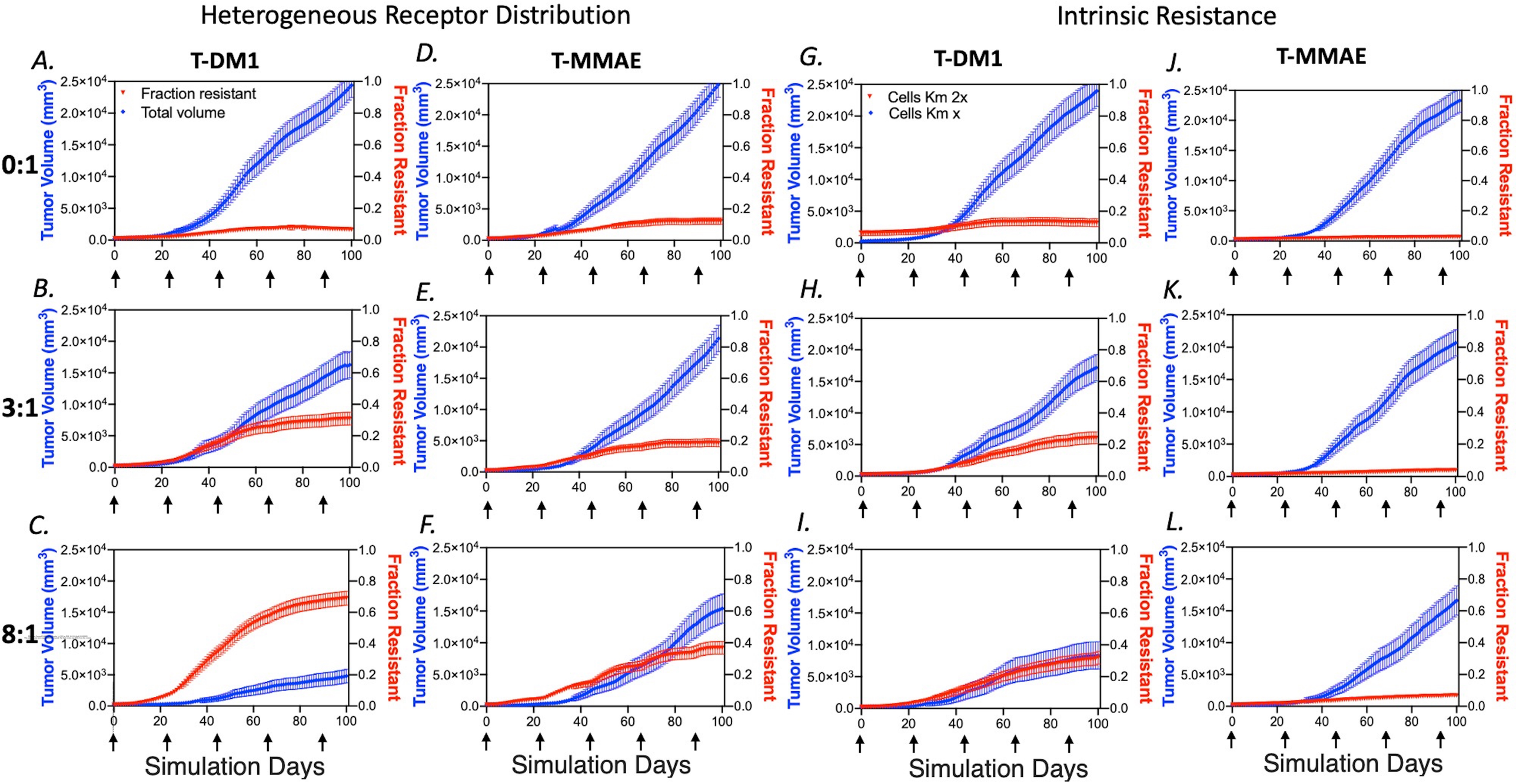
Heterogeneous Receptor Distribution
Intrinsic Resistance
A.
T-DM1
D.
T-MMAE
G.
T-DM1
J.
T-MMAE
Fraction resistant
Total volume
Cells Km 2x
Cells Km x
0:1
3:1
8:1
B.
E.
H.
K.
C.
F.
I.
L.
Tumor Volume (mm3)
Fraction Resistant
Simulation Days

Drug Metabolism and Disposition Manuscript DMD-AR-2021-000503

Supplemental Data: Simulating the Selection of Resistant Cells with Bystander Killing and Antibody Coadministration in Heterogeneous HER2 Position Tumors

Bruna Menezes[*], Jennifer Linderman[*#], and Greg M. Thurber[*#]

[*] Department of Chemical Engineering, University of Michigan, Ann Arbor, MI 48109

[#] Department of Biomedical Engineering, University of Michigan, Ann Arbor, MI 4810

Drug Metabolism and Disposition

Supplementary Data

Supplementary Tables – T1-2

1. Drug Dynamics Variables
2. Model Parameters

Supplementary Figures – S1-S7

1. Model schematic
2. Model fit to experimental blood vessel density
3. Calibration and validation of the ABM for T-DM1.
4. Calibration and validation of the ABM for T-MMAE.
5. Fractionated dosing with or without angiogenesis and comparison with experimental data
6. Distribution of T-DM1 and T-MMAE and their respective payloads at maximum uptake for same dose and DAR (3mg/kg and DAR3)
7. Percentage of tumors cell with concentration of payload bound with different bystander regimes

Supplementary Equations – (1-15)

References

Supplementary Tables

Table S.1 Drug Dynamics Variables

Variables	Unit	Description
ADC_c	nM	ADC in the central compartment
ADC_p	nM	ADC in the peripheral compartment
ADC or ADC_{tumor}	nM	Free ADC in the tumor
T_{free}	nM	Free Target
B_{ADC}	nM	ADC bound to Target
$B_{ADC,lys}$	nM	Bound ADC in the lysosome
P_{lys}	nM	Payload in the lysosome
P_{int}	nM	Payload not bound to intracellular target
P_b	nM	Payload bound to intracellular target
P_{ext}	nM	Payload free extracellular
Ab_{free}	nM	Free bare antibody
B_{Ab}	nM	Bare antibody bound to Target

Table S.2 Model Parameters

Parameter	Value	Unit	Description	Reference
k_{10}	4.55×10^{-6}	s^{-1}	Total antibody clearance	(Singh & Shah, 2019)
k_{12}	8.06×10^{-6}	s^{-1}	Antibody clearance for compartment 1 to 2	(Singh & Shah, 2019)
k_{21}	1.33×10^{-5}	s^{-1}	Antibody clearance for compartment 2 to 1	(Singh & Shah, 2019)
V_1	1.2×10^{-3}	L	Volume central compartment	(Menezes, Cilliers, Wessler, Thurber, & Linderman, 2020)
k_{on}	7.1×10^{5}	$M^{-1}s^{-1}$	ADC binding rate constant	(Bostrom, Haber, Koenig, Kelley, & Fuh, 2011)
K_d	0.5	nM	ADC equilibrium dissociation constant	(Bostrom et al., 2011)
k_{off}	3.5×10^{-4}	s^{-1}	ADC dissociation rate constant	(Bostrom et al., 2011)
k_e	3.3×10^{-5}	s^{-1}	ADC internalization rate constant	(Thurber, Zajic, & Wittrup, 2007)
k_{deg}	8×10^{-6}	s^{-1}	ADC lysosomal degradation rate constant	(Maass, Kulkarni, Betts, & Wittrup, 2016)
$k_{in,DM1}$	5.95×10^{-5}	s^{-1}	DM1 rate constant from the lysosome to cytosol	(Khera, Cilliers, Bhatnagar, & Thurber, 2018)
$k_{in,p\ DM1}$	5.95×10^{-5}	s^{-1}	DM1 cell internalization rate constant	(Khera et al., 2018)
$k_{out\ DM1}$	3.94×10^{-5}	s^{-1}	DM1 rate constant from the lysosome to cytosol	(Khera et al., 2018)
$k_{in,MMAE}$	1.41×10^{-3}	s^{-1}	MMAE rate constant from lysosome to cytosol	(Khera et al., 2018)
$k_{in,p\ MMAE}$	1.41×10^{-3}	s^{-1}	MMAE cell internalization rate constant	(Khera et al., 2018)
$k_{out\ MMAE}$	6.87×10^{-4}	s^{-1}	MMAE rate constant from lysosome to cytosol	(Khera et al., 2018)
$k_{on,p}$	8333	$M^{-1}s^{-1}$	DM1 and MMAE binding rate constant to intracellular target	(Singh et al., 2016)
$k_{off,p}$	0.003	s^{-1}	DM1 and MMAE unbinding rate constant	(Singh et al., 2016)
DAR_{DM1}	3.5	-	DM1 to antibody ratio	(Poon et al., 2013)
DAR_{MMAE}	4	-	MMAE to antibody ratio	(Singh & Shah, 2019)
R_s	2.75×10^{-11}	M/s	Target synthesis	(Thurber & Weissleder, 2011a)
T_{total}	5×10^{4} - 1×10^{6}	receptors/cell	Total surface targets per cell	Varied
P_{total}	20	uM	Total microtubule concentration per cell	(Khera et al., 2018)
ε	0.24	-	Void fraction of ADC and Ab	(Schmidt & Wittrup, 2009)
ε_{pay}	0.44	-	Void fraction of payload	(Bhatnagar, Deschenes, Liao, Cilliers, & Thurber, 2014; Khera et al., 2018)
D_{ADC}	1×10^{-11}	m^2/s	Effective Diffusivity of ADC and Ab	(Thurber & Weissleder, 2011b)
D_{DM1}	9.8×10^{-12}	m^2/s	Effective Diffusivity of DM1	(Khera et al., 2018)
D_{MMAE}	1.4×10^{-11}	m^2/s	Diffusivity of MMAE	(Khera et al., 2018)
P_{ADC}	3×10^{-9}	m /s	Vascular permeability of ADC and Ab	(Yuan, 1995)
P_{pay}	1×10^{-4}	m/s	Vascular permeability of the payload	(Thurber & Weissleder, 2011b)
$P_{max,\ DM1}$	0.0014	-	Maximum probability for cell killing for DM1	Calibrated
$K_{m,\ DM1}$	800	nM	Michaelis-Menten constant for DM1	Calibrated
$P_{max,\ MMAE}$	0.006	-	Maximum probability for cell killing for MMAE	Calibrated

$K_{m,\ MMAE}$	600	nM	Michaelis-Menten constant for MMAE	Calibrated
t_d (*in vivo*)	5-17	days	*In vivo* doubling time	Calibrated
t_d (*in vitro*)	1-2.5	days	*In vitro* doubling time	Estimated

*1 million receptors per cell corresponds to 833nM receptors where each cell occupies about 2x 10^{-12} L.

Supplemental Figures

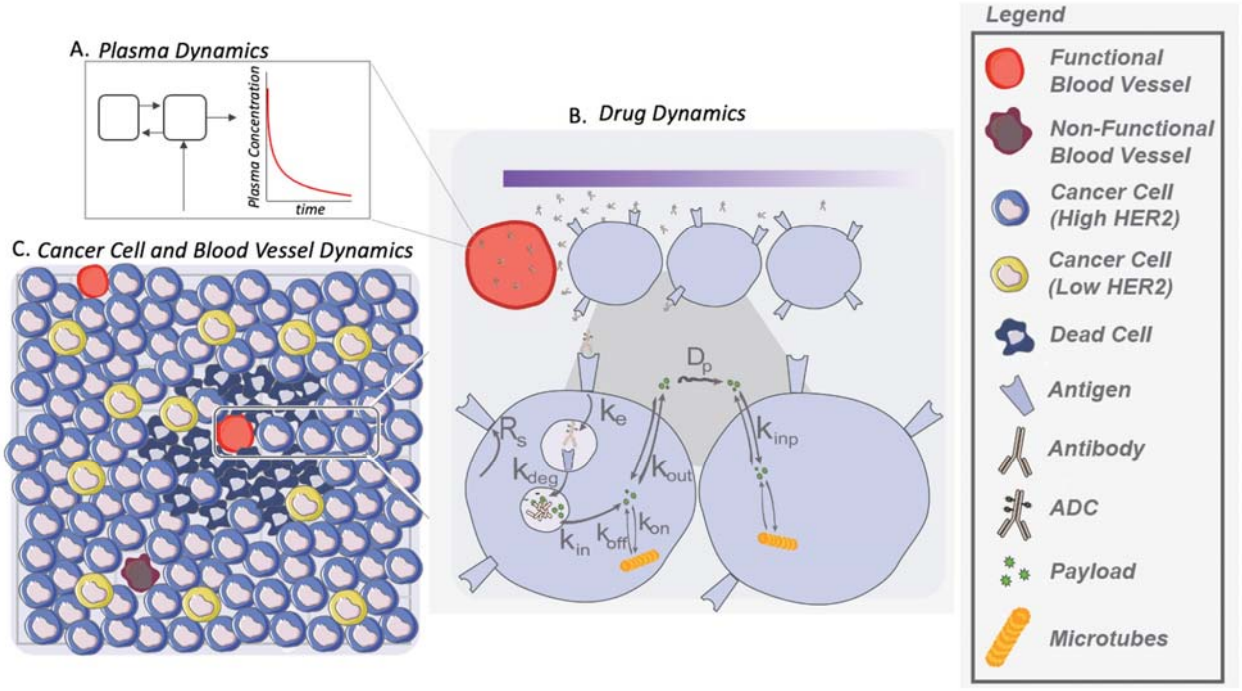

Figure S.1: Model schematic.
(A) Plasma dynamics are described with a two-compartment model (Eqs. S.1-2). (B) From the blood vessel, drugs enter the interstitial tissue (Eq. S.3 - Robin boundary condition), diffuse through it (Eq. S.4), and bind to HER2 receptors on cancer cells (Eq. S.5). There, ADCs are internalized and degraded. After the payloads DM1 and MMAE are released, they either bind to microtubules or escape the cancer cell. From the interstitial tissue, payloads diffuse and enter adjacent cells or intravasate into the blood vessels and wash out of the tumor (Eqs. S.6-14). (C) Cells with high or low receptor expression or sensitivity to drug, as well as blood vessels, behave based on the changes in the environment. All variables, parameters, and rate constants for model dynamics are shown in Table S.1 and Table S.2.

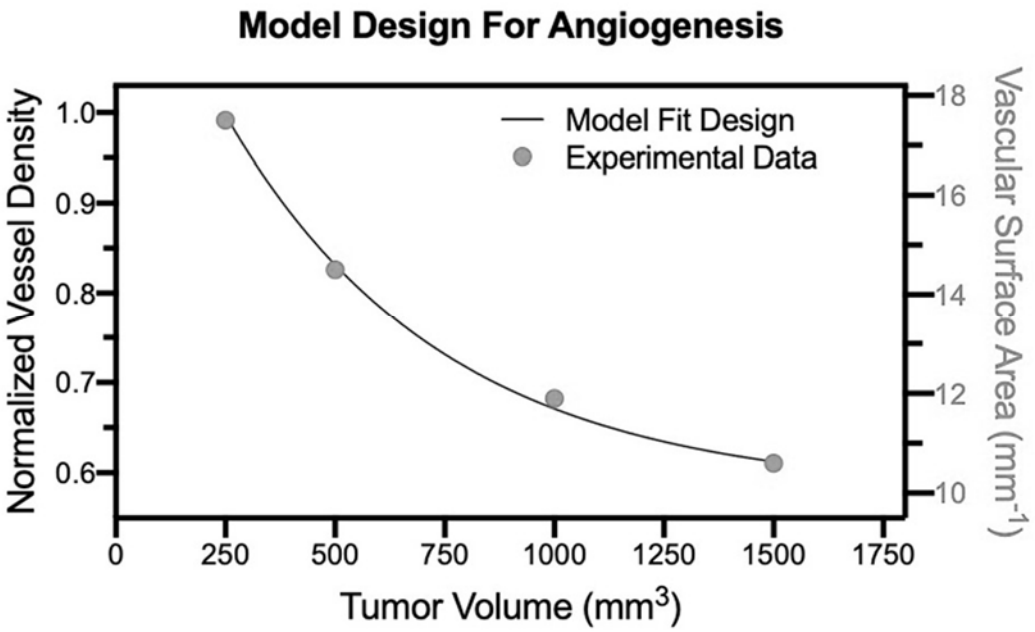

Figure S.2: Model fit to experimental blood vessel density.
The experimental data on vascular surface area (Hilmas & Gillette, 1974) show that blood vessel density decreases with an increase in the tumor volume. To account for this in the model, we used an exponential decay (Eq. 1). From the published experimental data, we considered the tumor volumes from 250 mm^3 to 1500 mm^3 and their respective decrease in vascular density. The new fraction of active blood vessel is then a function of the simulated tumor volume. As the tumor volume increases, the vascular density decreases following the rate shown here. At each agent time step, if the new fraction of active blood vessel is lower than the vessel density after the decrease is calculated, a randomly chosen blood vessel in the simulation becomes functional.

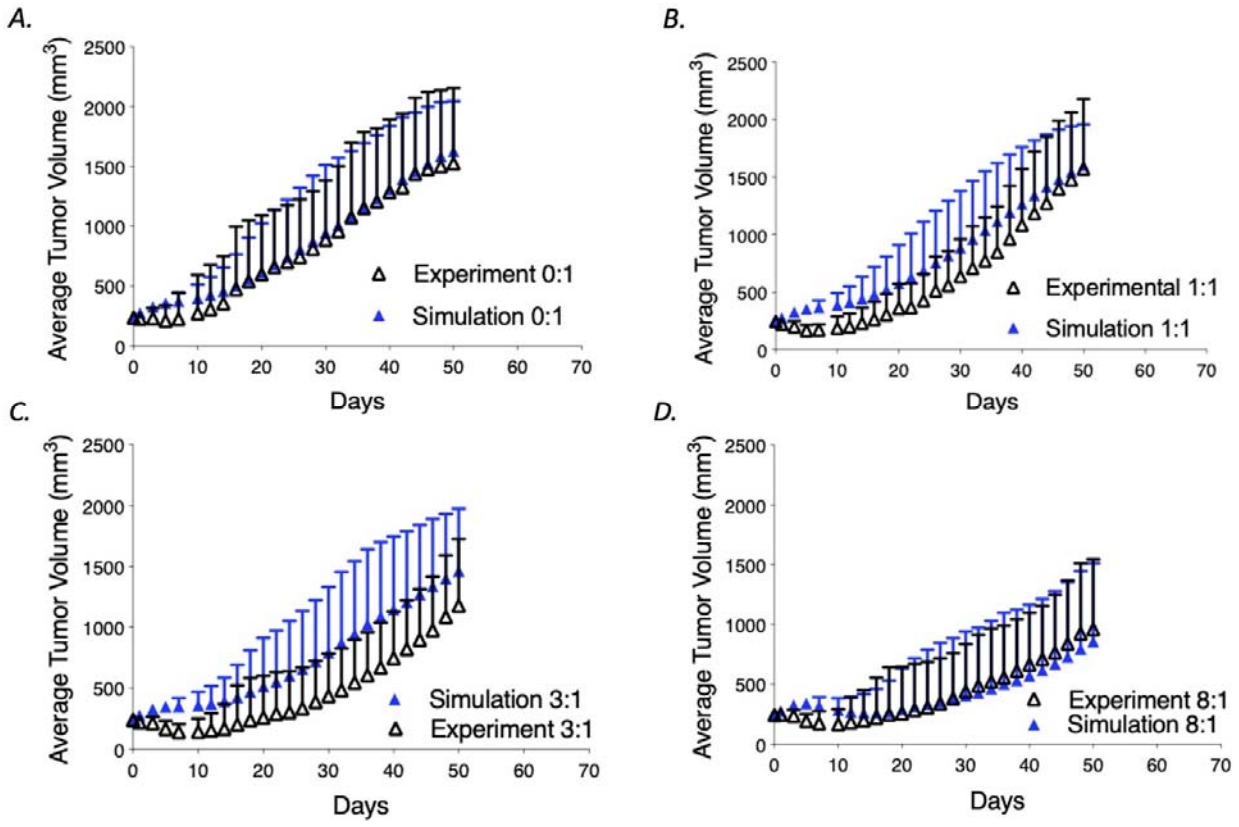

Figure S.3: Calibration and validation of the ABM for T-DM1.
(A) The model was calibrated to T-DM1 data based on the concentration payload bound to its target and to experimental data in (Cilliers, Menezes, Nessler, Linderman, & Thurber, 2018). In our original version of the model, we calibrated to the total concentration of the payload inside of the cell; the recalibration here allows delivery of T-DM1 to be described with the same framework as T-MMAE. Calibrated model parameter values (P_{max} and K_M for each payload) were fit using the response from ADC-only treatment (i.e. 0:1 ratio of trastuzumab to T-DM1) and are given in Table 2. (B-D) After fitting the cell sensitivity parameters P_{max} and K_M in A, the simulations were run with coadministration of the ADC with trastuzumab to compare with experimental results for model validation. The simulated efficacy of a constant ADC dose (3.6 mg/kg) combined with trastuzumab at a ratio of 1:1, 3:1, and 8:1 (trastuzumab to ADC ratio) shows similar efficacy as found experimentally (data from (Cilliers et al., 2018))

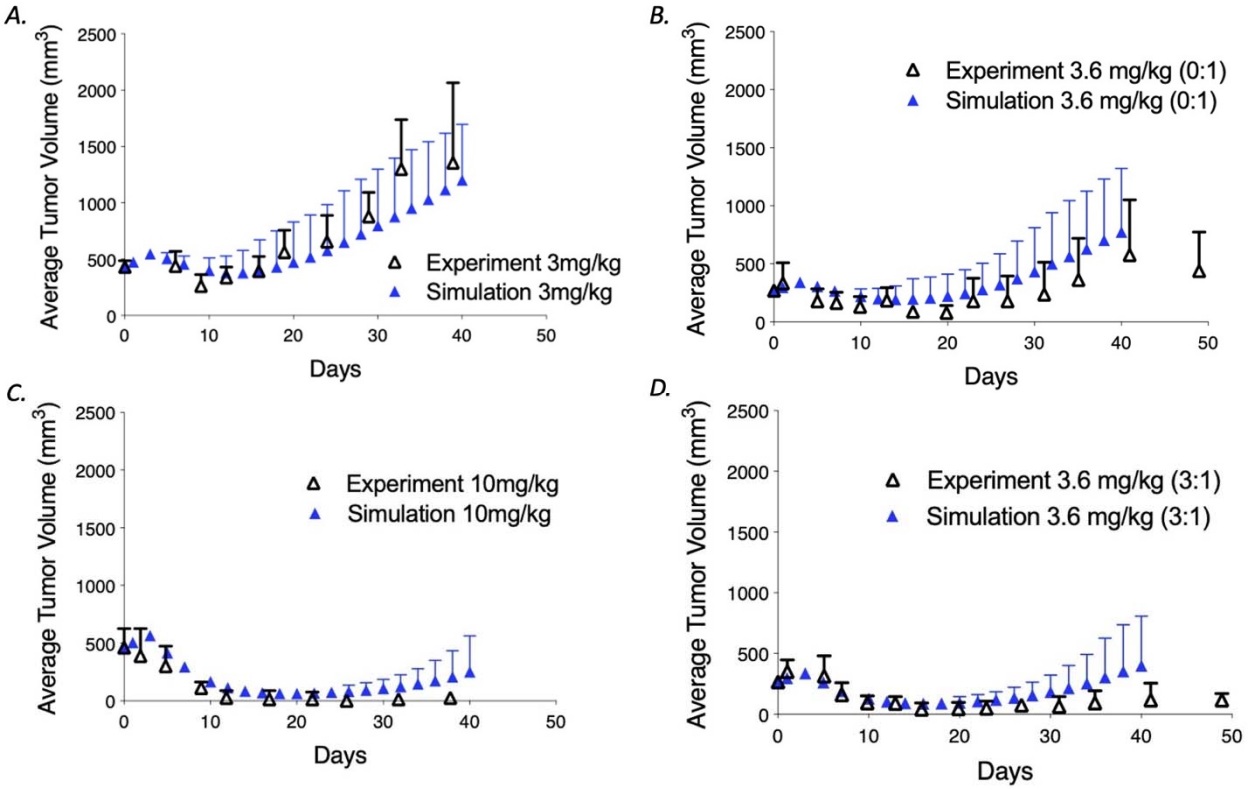

Figure S.4: Calibration and validation of the ABM for T-MMAE.
(A) The model was calibrated to T-MMAE using *in vivo* data from Singh *et al at 3mg/kg* (Singh, Seigel, et al., 2020). Two parameters were fit to calibrate the model: the P_{max} and K_M of MMAE, which are given in Table 2. (B-D) The model was run with doses of 10mg/kg ADC, 3.6mg/kg ADC, and 3.6 mg/kg with a 3:1 ratio of trastuzumab to ADC and compared to experimental data from (Singh, Guo, et al., 2020) for validation.

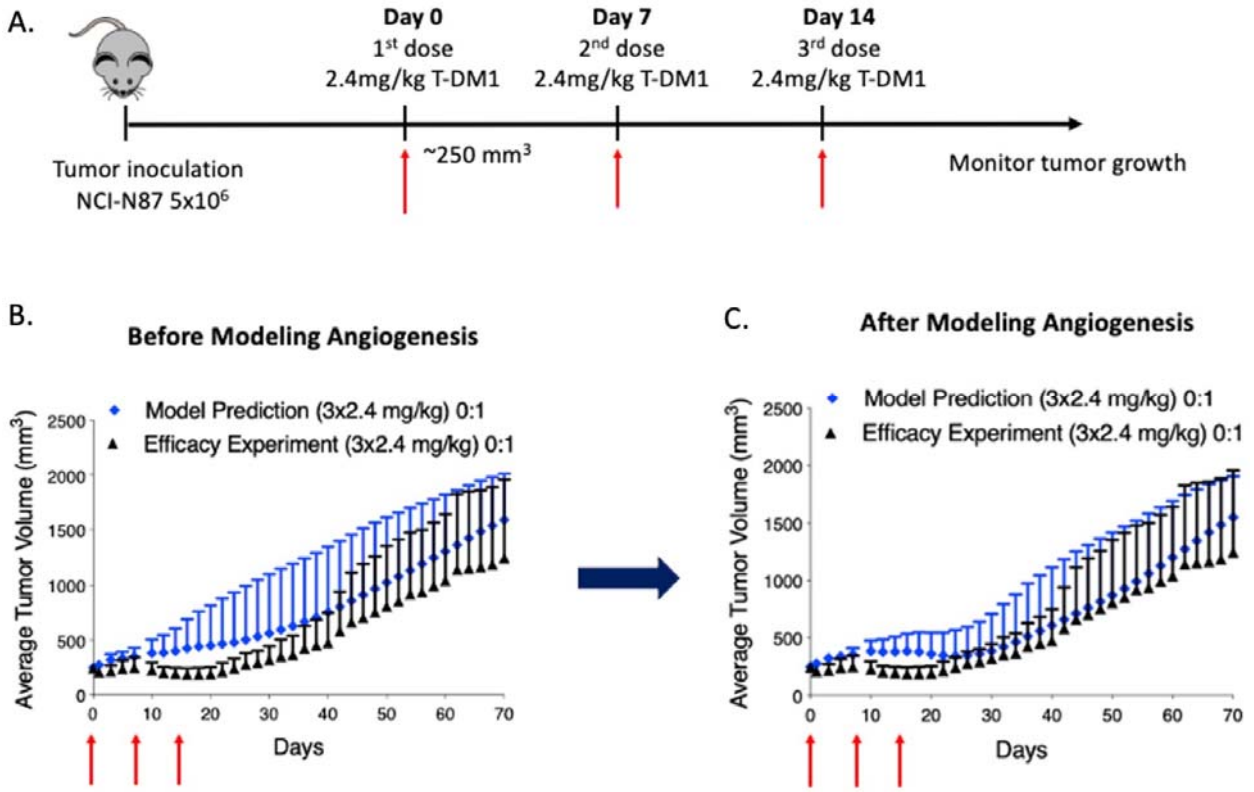

Figure S.5: Fractionated dosing with or without angiogenesis and comparison with experimental data.
(A) Using the experimental protocol from (Cilliers et al., 2018), 5 x 10^6 NCI-N87 cells were inoculated in the rear flank of nude mice. When the tumor reached approximated 250 mm^3, 3 doses of 2.4 mg/kg T-DM1 were given at days 0, 7, and 14. The tumor volume was measured every other day until 70 days or until it reached 2000 mm^3. (B-C) Simulations with the same doses and frequencies were performed before (Menezes et al., 2020) and after (this work) the addition of angiogenesis into the model. The inclusion of angiogenesis into the model better predicts tumor efficacy and tumor uptake.

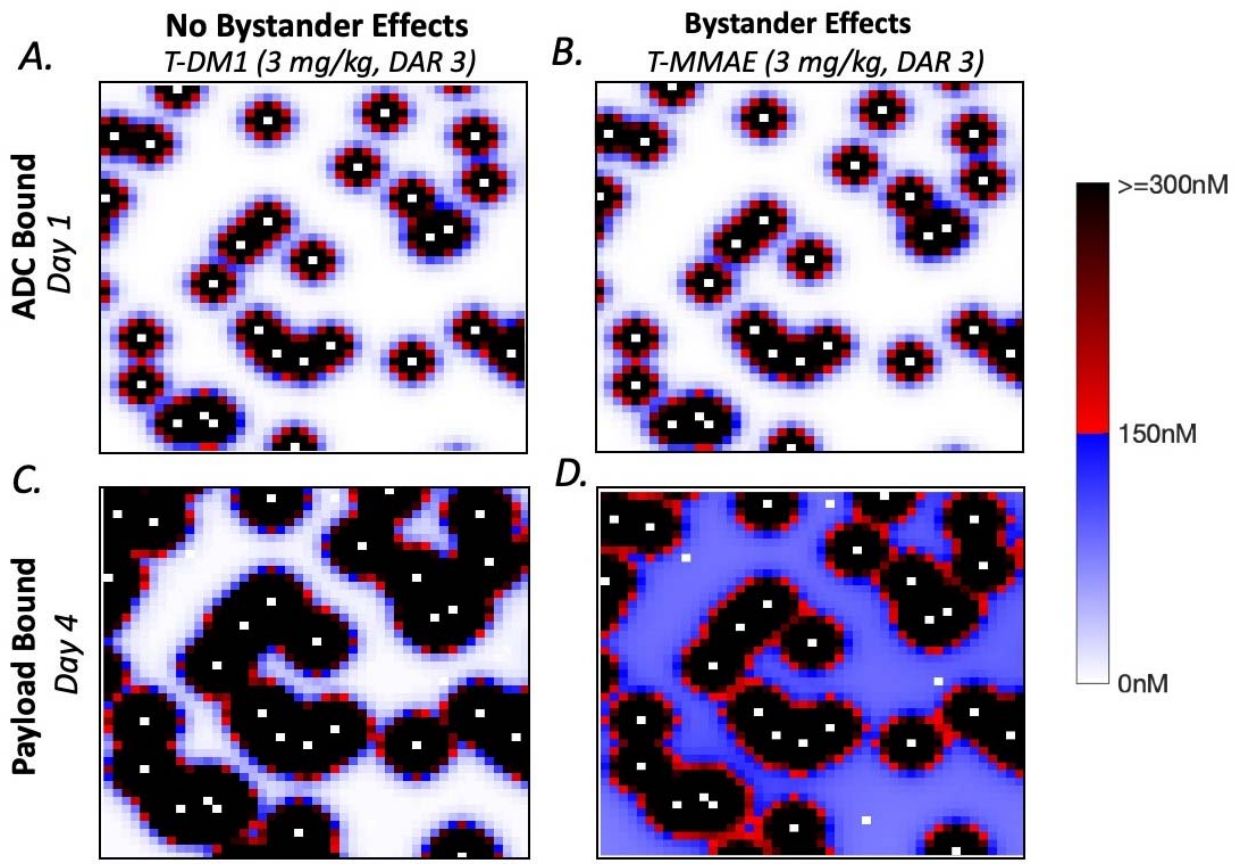

Figure S.6: Distribution of T-DM1 and T-MMAE and their respective payloads at maximum uptake for the same dose and DAR (3 mg/kg and DAR 3).
(A-B) Distribution of ADCs T-DM1 and T-MMAE (both 3 mg/kg with DAR 3) on the surface of the cells at 24 hrs showing the same ADC penetration from the matched antibody doses. (C-D) Distribution of microtubule-bound payload for DM1 and MMAE. Despite T-DM1 and T-MMAE having the same distribution on the surface of the cells, the MMAE payload diffuses deeper into the tissue to reach all cells with > 1 nM payload as seen in Fig.2.

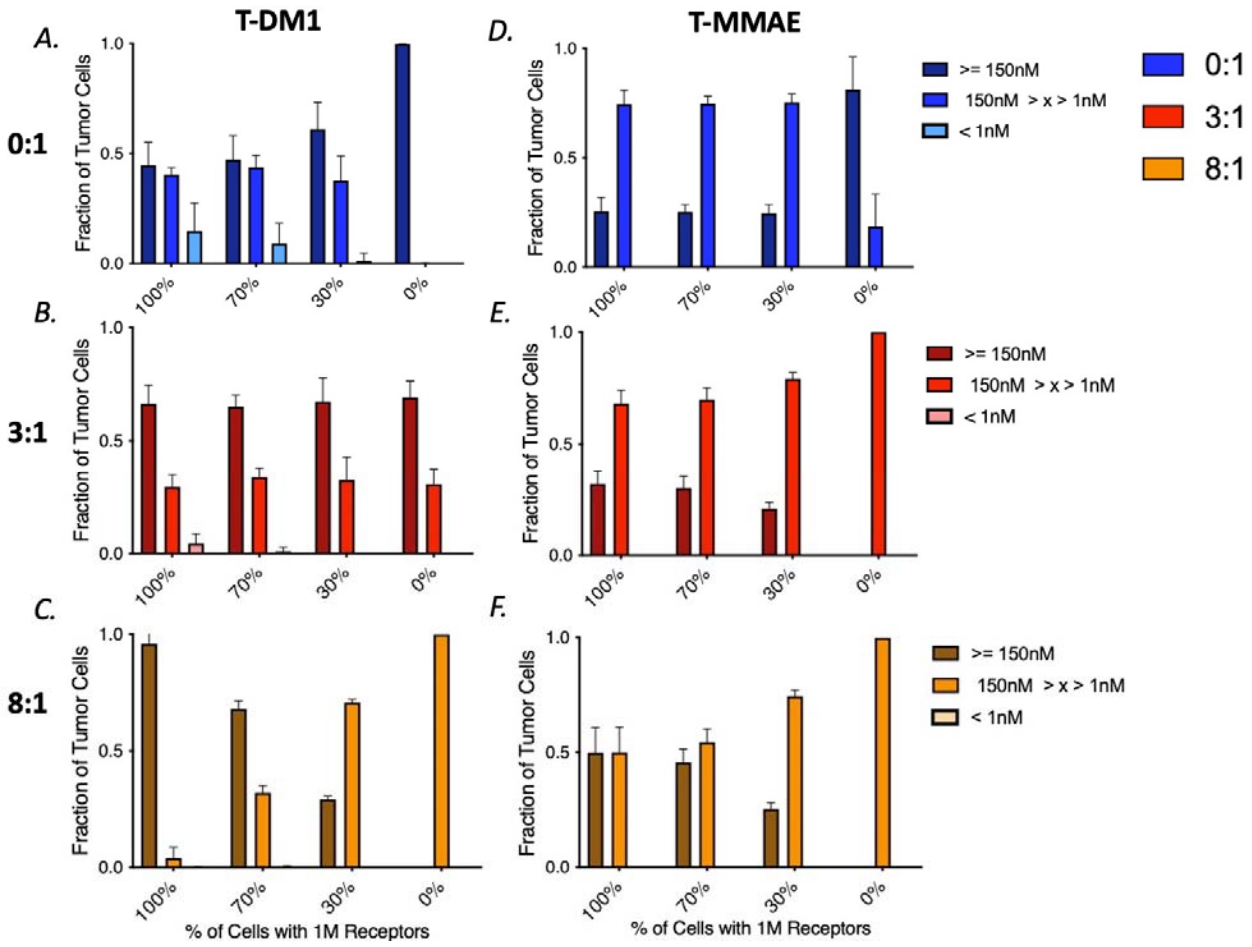

Figure S.7: Percentage of tumor cells with concentration of payload bound.
Percentage of tumor cells with concentrations greater or equal to 150nM, between 150nM and 1nM, and lower than 1nM for coadministration of T-DM1 (3.6 mg/kg and DAR 3.5) or T-MMAE (1.8 mg/kg and DAR 4) with trastuzumab. (A-C) Uptake of DM1 for coadministration of T-DM1 and trastuzumab for tumors with 100%, 70%, 30%, and 0% of cells with 1million receptors per cell vs 50 thousand receptors per cell. (D-F) Uptake of MMAE for coadministration of T-MMAE and trastuzumab for tumors with 100%, 70%, 30%, and 0% of cells with 1 million receptors per cell vs 50 thousand receptors per cell.

Model Equations

These model equations describe the plasma dynamics (using a biexponential compartment with no target-mediated drug disposition), extravasation and distribution in the grid (boundary conditions and diffusion), drug dynamics (intracellular processing for non-bystander and bystander payloads), and cell dynamics (e.g. cell division and cell death). More on this model can be found in (Menezes et al., 2020).

ADC plasma clearance:

$$\frac{\mathrm{d}[\mathrm{ADC}_c]}{\mathrm{dt}} = -k_{10}\,.\,[\mathrm{ADC}_c] - k_{12}\,.\,[\mathrm{ADC}_c] + k_{21}.[\mathrm{ADC_p}] \tag{S.1}$$

$$\frac{\mathrm{d}[\mathrm{ADC}_p]}{\mathrm{dt}} = -k_{21}.[\mathrm{ADC_p}] + k_{12}\,.\,[\mathrm{ADC}_c] \tag{S.2}$$

where the concentration of ADC at time zero is $ADC_c(0)$ = Dose/V_d (V_d is plasma volume of distribution) and $ADC_p(0) = 0$. The rate constants k_{12} and k_{21} were calibrated to account for the transport rate between the central and peripheral compartments ($k_{12} = CL_D / V_1$ and $k_{21} = CL_D/V_2$ where CL_D is the transport clearance between compartments and V_2 is the volume of the peripheral compartment). These rates are independent of binding in the tumor. Therefore, it is assumed there is negligible targeted mediated drug disposition (TMDD) in these simulations. (Mager & Jusko, 2001)

The boundary conditions at the blood vessels and at the edge of the tumor respectively are:

$$-\mathrm{D_{eff}}\frac{\mathrm{d[ADC]}}{\mathrm{dx}} = \mathrm{P}(\mathrm{ADC}_c - \frac{[ADC]_{tumor}}{\varepsilon}) \tag{S.3}$$

$$-\mathrm{D_{eff}}\frac{\mathrm{d[ADC]}}{\mathrm{dx}} = 0 \tag{S.4}$$

Diffusion of ADC in the tumor tissue is represented by the diffusion in the 2D cartesian coordinates:

$$\frac{\partial[ADC]}{\partial t} = D(\frac{\partial^2[ADC]}{\partial x^2} + \frac{\partial^2[ADC]}{\partial y^2}) \tag{S.5}$$

ADC dynamics in the cancer cells are described below:

$$\frac{d[ADC]}{dt} = -k_{on}\frac{[ADC]}{\varepsilon}.[T_{free}] + k_{off}[B_{ADC}] \tag{S.6}$$

$$\frac{d[T_{free}]}{dt} = R_s - k_{on}\frac{[ADC]}{\varepsilon}.[T_{free}] + k_{off}[B_{ADC}] - k_{on}\frac{[Ab_{free}]}{\varepsilon}.[T_{free}] + k_{off}[B_{Ab}] - k_e[T_{free}] \quad \text{(S.7)}$$

$$\frac{d[B_{ADC}]}{dt} = k_{on}\frac{[ADC]}{\varepsilon}.[T_{free}] - k_{off}[B_{ADC}] - k_e[B_{ADC}] \quad \text{(S.8)}$$

$$\frac{d[B_{ADC,lys}]}{dt} = k_e[B_{ADC}] - k_{deg}[B_{ADC,lys}] \quad \text{(S.9)}$$

$$\frac{d[P_{lys}]}{dt} = k_{deg}[B_{ADC,lys}]DAR - k_{in}[P_{lys}] \quad \text{(S.10)}$$

$$\frac{d[P_{int}]}{dt} = k_{in}[P_{lys}] + k_{in,p}\left(\frac{1-\varepsilon_p}{\varepsilon_p}\right)[P_{ext}] - k_{out,p}[P_{int}] - \frac{k_{on,p}}{(1-\varepsilon_p)(1+R)}\left(P_{target} - [P_b]\right)[P_{int}] + k_{off,p}[P_b] \quad \text{(S.11)}$$

$$\frac{d[P_b]}{dt} = \frac{k_{on,p}}{(1-\varepsilon_p)(1+R)}\left(P_{target} - [P_b]\right)[P_{int}] - k_{off,p}[P_b] \quad \text{(S.12)}$$

$$\frac{d[P_{ext}]}{dt} = -k_{in,p}\left(\frac{1-\varepsilon_p}{\varepsilon_p}\right)[P_{ext}] + k_{out,p}[P_{int}] \quad \text{(S.13)}$$

$$\frac{d[Ab_{free}]}{dt} = -k_{on}\frac{[Ab_{free}]}{\varepsilon}.[T_{free}] + k_{off}[B_{Ab}] \quad \text{(S.14)}$$

$$\frac{d[B_{Ab}]}{dt} = k_{on}\frac{[Ab_{free}]}{\varepsilon}.[T_{free}] - k_{off}[B_{Ab}] - k_e[B_{Ab}] \quad \text{(S.15)}$$

where R_s is receptor synthesis ($R_s = k_e \cdot T_{total}$) and $T_{free}(0) = T_{total}$.

Supplementary Data References

Bhatnagar, S., Deschenes, E., Liao, J., Cilliers, C., & Thurber, G. M. (2014). Multichannel Imaging to Quantify Four Classes of Pharmacokinetic Distribution in Tumors. *J Pharm Sci, 103*(10), 3276-3286. doi:10.1002/jps.24086

Bostrom, J., Haber, L., Koenig, P., Kelley, R. F., & Fuh, G. (2011). High affinity antigen recognition of the dual specific variants of herceptin is entropy-driven in spite of structural plasticity. *PLoS ONE, 6*(4), e17887. doi:10.1371/journal.pone.0017887

Cilliers, C., Menezes, B., Nessler, I., Linderman, J., & Thurber, G. M. (2018). Improved tumor penetration and single-cell targeting of antibody–drug conjugates increases anticancer efficacy and host survival. *Cancer Research, 78*(3), 758-768. doi:10.1158/0008-5472.Can-17-1638

Hilmas, D. E., & Gillette, E. L. (1974). Morphometric Analyses of the Microvasculature of Tumors During Growth and After X-irradiation. *Cancer, 33*(1), 103-110.

Khera, E., Cilliers, C., Bhatnagar, S., & Thurber, G. M. (2018). Computational transport analysis of antibody-drug conjugate bystander effects and payload tumoral distribution: implications for therapy. *Molecular Systems Design & Engineering, 3*(1), 73-88. doi:10.1039/c7me00093f

Maass, K. F., Kulkarni, C., Betts, A. M., & Wittrup, K. D. (2016). Determination of Cellular Processing Rates for a Trastuzumab-Maytansinoid Antibody-Drug Conjugate (ADC) Highlights Key Parameters for ADC Design. *AAPS J, 18*(3), 635-646. doi:10.1208/s12248-016-9892-3

Mager, D. E., & Jusko, W. J. (2001). General pharmacokinetic model for drugs exhibiting target-mediated drug disposition. *J Pharmacokinet Pharmacodyn, 28*(6), 507-532. Retrieved from http://www.ncbi.nlm.nih.gov/entrez/query.fcgi?cmd=Retrieve&db=PubMed&dopt=Citation&list_uids=11999290

Menezes, B., Cilliers, C., Wessler, T., Thurber, G. M., & Linderman, J. J. (2020). An Agent-Based Systems Pharmacology Model of the Antibody-Drug Conjugate Kadcyla to Predict Efficacy of Different Dosing Regimens. *AAPS J, 22*(2), 29. doi:10.1208/s12248-019-0391-1

Poon, K. A., Flagella, K., Beyer, J., Tibbitts, J., Kaur, S., Saad, O., . . . Reynolds, T. (2013). Preclinical safety profile of trastuzumab emtansine (T-DM1): mechanism of action of its cytotoxic component retained with improved tolerability. *Toxicol Appl Pharmacol, 273*(2), 298-313. doi:10.1016/j.taap.2013.09.003

Schmidt, M. M., & Wittrup, K. D. (2009). A modeling analysis of the effects of molecular size and binding affinity on tumor targeting. *Mol Cancer Ther, 8*(10), 2861-2871. doi:10.1158/1535-7163.MCT-09-0195

Singh, A. P., Guo, L., Verma, A., Wong, G. G., Thurber, G. M., & Shah, D. K. (2020). Antibody Coadministration as a Strategy to Overcome Binding-Site Barrier for ADCs: a Quantitative Investigation. *AAPS J, 22*(2), 28. doi:10.1208/s12248-019-0387-x

Singh, A. P., Maass, K. F., Betts, A. M., Wittrup, K. D., Kulkarni, C., King, L. E., . . . Shah, D. K. (2016). Evolution of Antibody-Drug Conjugate Tumor Disposition Model to Predict Preclinical Tumor Pharmacokinetics of Trastuzumab-Emtansine (T-DM1). *AAPS J, 18*(4), 861-875. doi:10.1208/s12248-016-9904-3

Singh, A. P., Seigel, G. M., Guo, L., Verma, A., Wong, G. G., Cheng, H. P., & Shah, D. K. (2020). Evolution of the Systems Pharmacokinetics-Pharmacodynamics Model for Antibody-Drug

Conjugates to Characterize Tumor Heterogeneity and In Vivo Bystander Effect. *J Pharmacol Exp Ther, 374*(1), 184-199. doi:10.1124/jpet.119.262287

Singh, A. P., & Shah, D. K. (2019). A “dual" cell-level systems PK-PD model to characterize the bystander effect of ADC. *J Pharm Sci*. doi:10.1016/j.xphs.2019.01.034

Thurber, G. M., & Weissleder, R. (2011a). Quantitating antibody uptake in vivo: conditional dependence on antigen expression levels. *Mol Imaging Biol, 13*(4), 623-632. doi:10.1007/s11307-010-0397-7

Thurber, G. M., & Weissleder, R. (2011b). A systems approach for tumor pharmacokinetics. *PLoS ONE, 6*(9), e24696. doi:10.1371/journal.pone.0024696

Thurber, G. M., Zajic, S. C., & Wittrup, K. D. (2007). Theoretic criteria for antibody penetration into solid tumors and micrometastases. *J Nucl Med, 48*(6), 995-999. Retrieved from http://www.ncbi.nlm.nih.gov/entrez/query.fcgi?cmd=Retrieve&db=PubMed&dopt=Citation&list_uids=17504872

Yuan, F. D., M. Fukumura, D. Leunig, M. Berk, D. Torchilin, V. Jain, R. K. . (1995). Vascular permeability in a human tumor xenograft: molecular size dependence and cutoff size. *Cancer Research, 55*, 3752-3756.